Stochastic Galerkin particle methods for kinetic equations of plasmas with uncertainties

Andrea Medaglia [a], Lorenzo Pareschi [b], Mattia Zanella [a],*

[a] *Department of Mathematics "F. Casorati", University of Pavia, Italy*
[b] *Department of Mathematics and Computer Science, University of Ferrara, Italy*

ARTICLE INFO

ABSTRACT

The study of uncertainty propagation is of fundamental importance in plasma physics simulations. To this end, in the present work we propose a novel stochastic Galerkin (sG) particle method for collisional kinetic models of plasmas under the effect of uncertainties. This class of methods is based on a generalized polynomial chaos (gPC) expansion of the particles' position and velocity. In details, we introduce a stochastic particle approximation for the Vlasov-Poisson system with a BGK term describing plasma collisions. A careful reformulation of such dynamics is needed to perform the sG projection and to obtain the corresponding system for the gPC coefficients. We show that the sG particle method preserves the main physical properties of the problem, such as conservations and positivity of the solution, while achieving spectral accuracy for smooth solutions in the random space. Furthermore, in the fluid limit the sG particle solver is designed to possess the asymptotic-preserving property necessary to obtain a sG particle scheme for the limiting Euler-Poisson system, thus avoiding the loss of hyperbolicity typical of conventional sG methods based on finite differences or finite volumes. We tested the schemes considering the classical Landau damping problem in the presence of both small and large initial uncertain perturbations, the two stream instability and the Sod shock tube problems under uncertainties. The results show that the proposed method is able to capture the correct behavior of the system in all test cases, even when the relaxation time scale is very small.
© 2023 The Authors. Published by Elsevier Inc. This is an open access article under the CC BY license (http://creativecommons.org/licenses/by/4.0/).

Contents

* Corresponding author.
E-mail address: mattia.zanella@unipv.it (M. Zanella).

1. Introduction

The construction of numerical methods in plasma physics described by kinetic equations is a challenging problem. The main difficulties arise both from the high dimensionality of the problem and from the formation of multiscale structures that must be captured by a numerical solver [3,4,9,13,17,18,23,45,51]. The numerical methods for plasma physics developed in the literature can be essentially divided into two groups: approaches based on direct discretizations of the corresponding system of partial differential equations (PDEs), like finite differences and finite volumes methods [13,17,18,41,51], and approaches based on approximations of the underlying particle dynamics at different levels, like particle-in-cell (PIC) methods [4–6,12,23,45]. Among the latter, Direct Simulation Monte Carlo (DSMC) methods allow an efficient solution of the kinetic system in the presence of collisions described by the Landau operator [3,16]. To the first group, in the collisional case, belong the Fourier spectral methods specifically designed for the fast solution of the Landau integral term [19,22,36].

The presence of uncertainty in the parameters of the physical model results in an additional computational challenge as it contributes to increasing the dimensionality of the system. Recently these kinds of problems have seen considerable effort by the scientific community and the introduction of numerous numerical techniques for quantifying the uncertainty [7,8,11, 15,20,28,33,39,48]. Among these techniques stochastic Galerkin methods based on generalized polynomial chaos expansions have shown the ability to achieve spectral accuracy in the random space for smooth solutions [27,49,50]. However, due to the intrusive nature of such approaches most physical properties are lost, among which physical conservations and positivity of the solution. In addition, as emphasized in [14,15], the system of coefficients defining the sG method may lead to loss of hyperbolicity for nonlinear systems of conservation laws. This is the case, in particular, of the fluid limit of the Vlasov-Poisson system for a collisional plasma leading to the Euler-Poisson system.

In this paper, following the methodology in [7,8,39,40] we introduce stochastic Galerkin particle methods for the Vlasov-Poisson system with a BGK collision term in presence of uncertainties. To this end we first introduce the particle approximation in absence of uncertainty and then, after generalizing the system to the case of uncertain inputs, we project the corresponding particle system into the space of orthogonal stochastic polynomials. As we shall see, this requires a careful reformulation of the particle dynamics. By construction, the resulting particle-based scheme preserves the main physical properties and the positivity of the reconstructed distribution function. Additionally, the use of a BGK collision term allows to achieve the asymptotic-preserving property in the fluid regime and to obtain a sG particle scheme for the limiting Euler-Poisson system that avoids the loss of hyperbolicity.

Previous results on sG schemes that avoid the loss of hyperbolicity have been based on suitable modifications of the gPC expansions [14,15,48] in a finite difference/volume setting. More precisely, in [15] an entropy closure method has been proposed, in [14] suitable conditions to preserve hyperbolicity have been derived, whereas in [48] an hybridization strategy between sG and stochastic collocation has been used. In our approach, instead, the problem is avoided thanks to the particle structure of the solution. We mention also recent results on uncertainty quantification in plasma physics obtained numerically in [11] and theoretically for the Landau damping in [21,43].

The rest of the manuscript is organized as follows. In the next section we introduce the Vlasov-Poisson system in presence of uncertainties and recall its fluid limit in the collisional case characterized by the Landau integral operator. A simplified collisional model based on the BGK operator is also introduced, which will later be used in the design of the numerical solver. Section 3 is then devoted to the detailed description of the numerical method. First the particle scheme in absence of uncertainties is presented and then it is generalized to the case of uncertain inputs through a stochastic Galerkin projection of the particle dynamics. In Section 4 several numerical results are reported, showing the ability of the method to achieve spectral accuracy for smooth solutions in the random space and to correctly capture the behavior of the solution in a series of prototypical test cases. Finally the paper ends with some concluding remarks and discussing future research directions.

2. Kinetic description of plasmas with uncertainties

We consider the evolution of the plasma electrons at the kinetic level described by [10]

$$\frac{\partial f(x, v, t, \mathbf{z})}{\partial t} + v \cdot \nabla_x f(x, v, t, \mathbf{z}) + E(x, t, \mathbf{z}) \cdot \nabla_v f(x, v, t, \mathbf{z}) = \frac{1}{\epsilon} Q(f, f)(x, v, t, \mathbf{z}), \tag{1}$$

where the one-particle distribution function $f(x, v, t, \mathbf{z})$ depends on position $x \in \mathbb{R}^3$, velocity $v \in \mathbb{R}^3$ and time $t > 0$, and $\epsilon > 0$ is the Knudsen number. The random vector $\mathbf{z} = (z_1, \ldots, z_d) \in \mathbb{R}^{d_z}$ characterizes the uncertainties of the system due, e.g., to missing information on the initial states, measurements of model parameters and boundary conditions. In the following we will suppose to know the distribution of $\mathbf{z}$, given by $p(\mathbf{z})$, i.e.

$$P(\mathbf{z} \in \Omega) = \int_{\Omega} p(\mathbf{z}) d\mathbf{z},$$

for any $\Omega \in \mathbb{R}^{d_z}$. In equation (1), $E(x, t, \mathbf{z})$ is the self-consistent electric field given by

$$E(x, t, \mathbf{z}) = -\nabla_x \phi(x, t, \mathbf{z}), \tag{2}$$

where $\phi(x, t, \mathbf{z})$ is the potential, solution to the Poisson equation

$$\Delta_x \phi(x, t, \mathbf{z}) = 1 - \int_{\mathbb{R}^3} f(x, v, t, \mathbf{z}) dv \tag{3}$$

subject to suitable boundary conditions. In (3) we have considered a uniform background of motionless positive ions.

The bilinear operator $Q(f, f)$ is the collisional operator describing the interactions between the charged particles. A classical choice is given by the Landau collision operator [29]

$$Q(f, f)(x, v, t, \mathbf{z}) = \nabla_v \cdot \int_{\mathbb{R}^3} \Phi(v - v_*) \big[\nabla_v f(v, \mathbf{z}) f(v_*, \mathbf{z}) - \nabla_{v_*} f(v_*, \mathbf{z}) f(v, \mathbf{z}) \big] dv_*,$$

where we omitted explicit dependence from (x, t) for brevity, and Φ is a 3×3 nonnegative symmetric matrix that defines the interactions between particles. Its usual form is given by

$$\Phi(v) = |v|^{\gamma+2} S(v), \qquad S(v) = I - \frac{v \otimes v}{|v|^2},$$

where $\gamma > 0$ in the case of hard potentials, $\gamma = 0$ in the Maxwellian case, and $\gamma < 0$ in the case of soft potential. In particular, the choice $\gamma = -3$ is the so-called Coulombian case and plays a central role in plasma physics. The kernel of the collision operator is characterized by local Maxwellian distributions

$$\mathcal{M}_{\rho, U, T}(x, v, \mathbf{z}) = \rho(x, \mathbf{z}) \left(\frac{1}{2\pi T(x, \mathbf{z})} \right)^{\frac{3}{2}} \exp\left(-\frac{(v - U(x, \mathbf{z}))^2}{2T(x, \mathbf{z})} \right), \tag{4}$$

where we introduced the mass, the momentum and temperature as

$$\rho(x, \mathbf{z}) = \int_{\mathbb{R}^3} f(x, v, t, \mathbf{z}) dv,$$

$$\rho(x, \mathbf{z}) U(x, \mathbf{z}) = \int_{\mathbb{R}^3} v f(x, v, t, \mathbf{z}) dv,$$

$$T(x, \mathbf{z}) = \frac{1}{3\rho(x, \mathbf{z})} \int_{\mathbb{R}^3} |v - U(x, \mathbf{z})|^2 f(x, v, t, \mathbf{z}) dv.$$

In the collisionless case $\epsilon \to +\infty$ from (1) we recover the Vlasov-Poisson model, whereas passing formally to the limit $\epsilon \to 0$ we obtain $f = \mathcal{M}_{\rho, U, T}$ and thus, defining

$$W(x, \mathbf{z}) = \rho(x, \mathbf{z}) \left(\frac{|U(x, \mathbf{z})|^2}{2} + \frac{3T(x, \mathbf{z})}{2} \right), \quad p(x, \mathbf{z}) = \rho(x, \mathbf{z}) T(x, \mathbf{z}),$$

we recover the Euler-Poisson system

$$\partial_t \rho + \nabla_x \cdot (\rho U) = 0$$
$$\partial_t (\rho U) + \nabla_x \cdot (\rho U \otimes U) + \nabla_x p = \rho \nabla_x \varphi$$
$$\partial_t W + \nabla_x \cdot ((W + p) U) = \rho U \cdot \nabla_x \varphi \tag{5}$$
$$\Delta_x \varphi = \rho - 1,$$

where we omitted the dependence from the uncertainty and the physical variables for the sake of simplicity.

In this work, following usual approximations of collisional processes, we consider a BGK-type collisional operator [1,2]

$$Q\left(f, \mathcal{M}\right)(x, v, t, \mathbf{z}) = \mu(\mathcal{M}_{\rho, U, T}(x, v, \mathbf{z}) - f(x, v, t, \mathbf{z})), \tag{6}$$

with $\mu > 0$ the collision frequency. Recent approaches to plasma dynamics involving BGK-type operators have been proposed in [12,30,48].

For the numerical solution of (1) with uncertainties several approaches have been proposed in the literature [11,27,48]. In most cases, however, when an intrusive method like stochastic-Galerkin is adopted, most physical properties are lost and a particular care is required to avoid the loss of hyperbolicity of the solution in fluid regimes [14,15,48]. In the sequel, we will consider a different approach to the problem based on a stochastic-Galerkin projection of the corresponding particle approximation.

3. The stochastic Galerkin particle method

In this section, we first recall particle methods for the numerical approximation of equation (1) in absence of uncertainties. Without attempting to review the very huge literature on particle methods for kinetic equations, we mention Direct Simulation Monte Carlo (DSMC) [34,35,37,38] and particle-in-cell (PIC) methods for collisionless plasmas, see e.g. [9,23] and the references therein. It is worth to mention that extensive efforts have been devoted also to deterministic methods, see e.g. [3,13,16–18,24,25,45,51] and the references therein.

Furthermore, we focus on fundamentals of stochastic Galerkin methods and we derive the corresponding sG particle approach. We highlight that these methods have been previously studied for mean-field models of collective phenomena [7,8,32], and subsequently extended to the space-homogeneous Boltzmann equation [39].

3.1. The particle based method in a deterministic setting

To introduce the particle method, we first consider equation (1) without uncertainties. We are interested in the evolution of the density $f = f(x, v, t)$, $x, v \in \mathbb{R}^3$, $t \geq 0$, solution to (1) and complemented with the initial condition $f(x, v, 0) = f_0(x, v)$. Let us consider a time discretization of the interval $[0, T_f]$ of size $\Delta t > 0$. Denoting by $f^n(x, v)$ an approximation of $f(x, v, t^n)$, with $t^n = n\Delta t$, the starting point is a splitting between the numerical solution of the BGK collision step $f^* = \mathcal{C}_{\Delta t}(f^n)$

$$\begin{cases} \dfrac{\partial f^*}{\partial t} = \dfrac{1}{\varepsilon} Q\left(f^*, \mathcal{M}_{\rho, U, T}\right), \\ f^*(x, v, 0) = f^n(x, v), \end{cases} \tag{7}$$

and the Vlasov transport step $f^{**} = \mathcal{T}_{\Delta t}(f^*)$

$$\begin{cases} \dfrac{\partial f^{**}}{\partial t} + v \cdot \nabla_x f^{**} + E(x, t) \cdot \nabla_v f^{**} = 0, \\ f^{**}(x, v, 0) = f^*(x, v, \Delta t). \end{cases} \tag{8}$$

The solution at the time t^{n+1} is therefore given by the first order splitting method

$$f^{n+1}(x, v) = \mathcal{T}_{\Delta t}\left(\mathcal{C}_{\Delta t}(f^n)(x, v)\right).$$

Higher order methods can be considered, such as the second order Strang splitting scheme [46]

$$f^{n+1}(x, v) = \mathcal{C}_{\Delta t/2}\left(\mathcal{T}_{\Delta t}\left(\mathcal{C}_{\Delta t/2}(f^n)(x, v)\right)\right).$$

It should be noted, however, that close to fluid regimes the above Strang splitting degenerates to first order accuracy. This drawback can be avoided using suitable IMEX Runge-Kutta techniques which up to date are not available for particle based solvers [19].

To reconstruct the distribution function at each time step several approaches are possible. Possible approaches are represented by constructing a histogram of position and velocities of the set of particles in the phase space, by the weighted rule, where each particle is counted in a computational cell and in neighboring cells with a fractions that is proportional to the overlapping area, or by reconstruction techniques based on a convolution of empirical distribution with a suitable mollifier, see e.g. [26]. In particular, in the following, we adopt the histogram reconstruction. We approximate the distribution function at each time step n with a sample of N particles $\{x_i^n, v_i^n\}_{i=1}^N$

$$f_N^n(x, v) = \frac{m}{N} \sum_{i=1}^N \delta(x - x_i^n) \otimes \delta(v - v_i^n),$$

being $\delta(\cdot)$ a Dirac delta and $m = \int_{\mathbb{R}^3} \rho(x)dx$ the total mass. We observe that the weight $\omega = m/N$ is shared by each particle, it does not influence the dynamics but it should be taken into account in the reconstruction. The particles are then advanced in time by solving the equations of motion derived from (7) and (8). In the following, we describe the BGK collisional step and the transport step separately.

Collision step. In order to present the algorithm for the BGK collision step, we rewrite (7) at discrete time steps Δt as

$$f^*(x, v) = \left(1 - e^{-\nu \Delta t}\right) \mathcal{M}_{\rho, U, T}(x, v) + e^{-\nu \Delta t} f^n(x, v),$$

where $\nu = \mu/\epsilon$. From a particle point of view, we can interpret the previous relation in a simple probabilistic setting, see [34,35]. With a probability $\left(1 - e^{-\nu \Delta t}\right)$, at the time step n, a particle (x_i^n, v_i^n) is replaced by a particle with position and velocity sampled from the local Maxwellian $\mathcal{M}_{\rho, U, T}$. Whereas, with probability $e^{-\nu \Delta t}$ the particle maintains its state.

The previous local quantities are computed with a piecewise constant approach. Let us consider N_ℓ equally spaced cells I_ℓ of a one-dimensional spatial domain $I \subset \mathbb{R}$ so that $\cup_{\ell=1}^{N_\ell} I_\ell = I$ and $I_\ell \cap I_k = \varnothing$ for $\ell \neq k$. Then, at time t^n, mass, momentum and temperature are computed as

$$\rho_\ell^n = \frac{m}{N} \sum_{i=1}^{N} \chi(x_i^n \in I_\ell),$$

$$U_\ell^n = \frac{m}{\rho_\ell N} \sum_{i=1}^{N} v_i^n \chi(x_i^n \in I_\ell), \tag{9}$$

$$T_\ell^n = \frac{m}{\rho_\ell N} \sum_{i=1}^{N} (v_i^n - U_\ell^n)^2 \chi(x_i^n \in I_\ell),$$

being $\chi(\cdot)$ is the indicator function. Hence, we may rewrite the BGK collisional process for every $i = 1, \ldots, N$ in a compact form as follows

$$v_i^{n+1} = \chi\left(\xi < e^{-\nu \Delta t}\right) v_i^n + \left(1 - \chi\left(\xi < e^{-\nu \Delta t}\right)\right) \sum_{\ell=1}^{N_\ell} \chi\left(x_i^n \in I_\ell\right) \left(U_\ell^n + \tilde{v}_i \sqrt{T_\ell^n}\right) \tag{10}$$

being $\xi \sim \mathcal{U}([0, 1])$ and $\tilde{v}_i \sim \mathcal{N}(0, 1)$ a standard normally distributed random variable. In order to preserve the moments in each cell, we compute the samples $\{\tilde{v}_i\}_{i=1}^{N}$ according to [38]. Let

$$\tilde{V} = \frac{1}{N} \sum_{i=1}^{N} \tilde{v}_i \qquad \tilde{E} = \frac{1}{2N} \sum_{i=1}^{N} \tilde{v}_i^2$$

be mean and energy of the sampled particles. We further rescale the samples to guarantee zero mean $u = 0$ and energy $e = 1/2$, that is

$$\frac{1}{N} \sum_{i=1}^{N} \frac{\tilde{v}_i - \lambda}{\tau} = u \qquad \frac{1}{2N} \sum_{i=1}^{N} \left(\frac{\tilde{v}_i - \lambda}{\tau}\right)^2 = e, \tag{11}$$

where

$$\tau^2 = \frac{\tilde{E} - \tilde{V}/2}{e - u/2} \qquad \lambda = \tilde{V} - \tau u.$$

As observed in [38] the above scaling $\tilde{v}_i \to (\tilde{v}_i - \lambda)/\tau$ being a linear transformation does not alter the normal distribution of the particle samples and, by construction, preserves momentum and energy in each cell.

Algorithm 1 BGK collision step.

- Compute the initial position and velocity of the particles $\{x_i^0, v_i^0\}_{i=1}^{N}$ by sampling from the initial distribution $f^0(x, v)$;
- compute the velocities $\{\tilde{v}_i\}_{i=1}^{N}$ by sampling a standard normal distribution $\mathcal{N}(0, 1)$ according to (11);
- for $n = 0$ to $n_{\text{TOT}} - 1$, given $\{x_i^n, v_i^n\}_{i=1}^{N}$:
  – compute ρ_ℓ^n, U_ℓ^n, T_ℓ^n in each cell I_ℓ, $\ell = 1, \ldots, N_\ell$, according to (9);
  – for every particle $i = 1, \ldots, N$:
    * select ξ uniformly in $[0, 1]$;
    * compute the post interaction velocities v_i^{n+1} according to (10);
- end for.

Vlasov transport step. The equations of motion of the particles obtained from (8) are the following coupled set of ODEs:

$$\frac{dx_i(t)}{dt} = v_i(t), \qquad \frac{dv_i(t)}{dt} = E(x_i, t),$$ (12)

that can be solved on the computational domain through the following three steps method complemented with boundary conditions.

Let $\{x_i^n, v_i^n\}_{i=1}^N$ be at the time step n and we indicate with $E_\ell^{n+1/2}$ the electric field in the cell I_ℓ at the step $n + 1/2$. We consider the following splitting approach

$$x_i^{n+1/2} = x_i^n + v_i^n \frac{\Delta t}{2},$$ (13)

$$v_i^{n+1} = v_i^n + \Delta t \sum_{\ell=1}^{N_\ell} E_\ell^{n+1/2} \chi(x_i^{n+1/2} \in I_\ell),$$ (14)

$$x_i^{n+1} = x_i^{n+1/2} + v_i^{n+1} \frac{\Delta t}{2}.$$ (15)

The electric field in (14) is computed by solving the Poisson equation for the potential (3) with a mesh based method on a uniform grid. To this end, we compute as in (9) the local mass on the uniform grid at time $n + 1/2$. The process can be summarized as follows.

Remark 1. The PIC-type scheme (13)-(15) evolves each sample through the splitting strategy defined in [45] to each sample, thus it conserves mass and momentum. The mass is conserved if no particle gets in or out of the domain, since the total mass m is constant in time and does not affect the dynamics. The total momentum is conserved provided the Poisson solver is such that at the discrete level

$$\int_I E(x)\rho(x)dx = 0,$$ (16)

see Proposition 10 in [45], Section 3.2.2. This condition is met on a periodic domain. Methods satisfying this condition can be found, e.g., in Section 4.2 of the same work.

Algorithm 2 Vlasov transport step.

- Compute the initial position and velocity of the particles $\{x_i^0, v_i^0\}_{i=1}^N$ by sampling from initial distribution $f^0(x, v)$;
- for $n = 0$ to $n_{\text{TOT}} - 1$, given $\{x_i^n, v_i^n\}_{i=1}^N$:
  - compute the free transport on $\frac{\Delta t}{2}$ according to (13), and apply the boundary conditions;
  - compute the mass $\rho^{n+1/2}$ and then the electric field in each cell $\{E_\ell^{n+1/2}\}_{\ell=1}^{N_\ell}$ by solving the Poisson equation with a mesh based method satisfying condition (16);
  - update the velocities on Δt according to (14)
  - compute the free transport on $\frac{\Delta t}{2}$ according to (15), and apply the boundary conditions;
- end for.

3.2. Stochastic Galerkin particle based methods

We consider stochastic Galerkin expansion of Algorithms 1-2 for the numerical approximation of (1) with uncertainties. We consider a sample of N particles $x_i(t^n, \mathbf{z})$, $v_i(t^n, \mathbf{z})$, $i = 1, \ldots, N$ at time $t^n = n\Delta t$, and we expand them by their generalized polynomial chaos (gPC) expansion

$$x_i^n(\mathbf{z}) \approx x_i^{n,M}(\mathbf{z}) = \sum_{h=0}^M \hat{x}_{i,h}^n \Psi_h(\mathbf{z}),$$

$$v_i^n(\mathbf{z}) \approx v_i^{n,M}(\mathbf{z}) = \sum_{h=0}^M \hat{v}_{i,h}^n \Psi_h(\mathbf{z}),$$ (17)

being $\{\Psi_h(\mathbf{z})\}_{h=0}^M$ a set of polynomials of degree less or equal to $M \in \mathbb{N}$, orthonormal with respect to the measure $p(\mathbf{z})d\mathbf{z}$

$$\int_\Omega \Psi_h(\mathbf{z})\Psi_k(\mathbf{z})p(\mathbf{z})d\mathbf{z} = \mathbb{E}_{\mathbf{z}}[\Psi_h(\cdot)\Psi_k(\cdot)] = \delta_{hk},$$

where $\Omega \in \mathbb{R}^d$ and δ_{hk} is the Kronecker delta. The polynomials $\{\Psi_h(\mathbf{z})\}_{h=0}^M$ are chosen following the so-called Wiener–Askey scheme [49,50], depending on the distribution of the parameters. In (17), for fixed $h = 0, \ldots, M$, the terms $\hat{x}_{i,h}^n$ and $\hat{v}_{i,h}^n$ are the projections of the positions and velocities respectively in the space generated by the polynomial of degree $h \geq 0$

$$
\begin{aligned}
\hat{x}_{i,h}^n &= \int_{\Omega} x_i^n(\mathbf{z}) \Psi_h(\mathbf{z}) p(\mathbf{z}) d\mathbf{z} = \mathbb{E}_{\mathbf{z}}[x_i^n(\cdot)\Psi_h(\cdot)], \\
\hat{v}_{i,h}^n &= \int_{\Omega} v_i^n(\mathbf{z}) \Psi_h(\mathbf{z}) p(\mathbf{z}) d\mathbf{z} = \mathbb{E}_{\mathbf{z}}[v_i^n(\cdot)\Psi_h(\cdot)].
\end{aligned}
\tag{18}
$$

Stochastic collision step. To define the sG particle algorithm of the BGK step with random inputs we consider a projection on the polynomial space defined by the uncertainties of the collision process in Section 3.1. Therefore, if we consider the discretization in N_ℓ cells as before, we compute at each time step t^n uncertain mass, mean velocity and temperature as

$$
\begin{aligned}
\rho_\ell^n(\mathbf{z}) &= \frac{m(\mathbf{z})}{N} \sum_{i=1}^N \chi(x_i^n(\mathbf{z}) \in I_\ell), \\
U_\ell^n(\mathbf{z}) &= \frac{m(\mathbf{z})}{\rho_\ell^n(\mathbf{z})N} \sum_{i=1}^N v_i^n(\mathbf{z})\chi(x_i^n(\mathbf{z}) \in I_\ell), \\
T_\ell^n(\mathbf{z}) &= \frac{m(\mathbf{z})}{\rho_\ell^n(\mathbf{z})N} \sum_{i=1}^N (v_i^n(\mathbf{z}) - U_\ell^n(\mathbf{z}))^2 \chi(x_i^n(\mathbf{z}) \in I_\ell),
\end{aligned}
\tag{19}
$$

that are approximated through the gPC particles' expansion as

$$
\begin{aligned}
\rho_\ell^{n,M}(\mathbf{z}) &= \frac{m(\mathbf{z})}{N} \sum_{i=1}^N \chi(x_i^{n,M}(\mathbf{z}) \in I_\ell), \\
U_\ell^{n,M}(\mathbf{z}) &= \frac{m(\mathbf{z})}{\rho_\ell^{n,M}(\mathbf{z})N} \sum_{i=1}^N v_i^{n,M}(\mathbf{z})\chi(x_i^{n,M}(\mathbf{z}) \in I_\ell), \\
T_\ell^{n,M}(\mathbf{z}) &= \frac{m(\mathbf{z})}{\rho_\ell^{n,M}(\mathbf{z})N} \sum_{i=1}^N (v_i^{n,M}(\mathbf{z}) - U_\ell^{n,M}(\mathbf{z}))^2 \chi(x_i^{n,M}(\mathbf{z}) \in I_\ell),
\end{aligned}
\tag{20}
$$

where $m(\mathbf{z}) = \int \rho(x, \mathbf{z})dx$ is the uncertain total mass. We substitute into (10) the gPC expansion $x_i^{n,M}(\mathbf{z})$, $v_i^{n,M}(\mathbf{z})$ of the particles

$$
\begin{aligned}
v_i^{n+1,M} = &\chi\left(\xi < e^{-\nu\Delta t}\right) v_i^{n,M} \\
&+ \left(1 - \chi\left(\xi < e^{-\nu\Delta t}\right)\right) \sum_{\ell=1}^{N_\ell} \chi\left(x_i^{n,M} \in I_\ell\right) \left(U_\ell^{n,M} + \tilde{v}_i\sqrt{T_\ell^{n,M}}\right).
\end{aligned}
\tag{21}
$$

Hence, the projection of (21) on the linear space, for each $h = 0, \ldots, M$, is given by

$$
\hat{v}_{i,h}^{n+1} = \chi\left(\xi < e^{-\nu\Delta t}\right) \hat{v}_{i,h}^n + \left(1 - \chi\left(\xi < e^{-\nu\Delta t}\right)\right) \sum_{\ell=1}^{N_\ell} \hat{W}_{i,h}^{n,\ell},
\tag{22}
$$

with the collision matrix

$$
\hat{W}_{i,h}^{n,\ell} = \int_{\Omega} \chi\left(x_i^{n,M}(\mathbf{z}) \in I_\ell\right) \left(U_\ell^{n,M}(\mathbf{z}) + \tilde{v}_i\sqrt{T_\ell^{n,M}(\mathbf{z})}\right) \Psi_h(\mathbf{z}) p(\mathbf{z}) d\mathbf{z}
\tag{23}
$$

and where $\tilde{v}$ is a random variable with normal distribution as before.

The integral in (23) may be computed through standard Gaussian quadrature. For example, for a one-dimensional uncertainty using K nodes we have

$$
\hat{W}_{i,h}^{n,\ell} \approx \sum_{k=1}^K w_k \chi\left(x_i^{n,M}(z_k) \in I_\ell\right) \left(U_\ell^{n,M}(z_k) + \tilde{v}_i\sqrt{T_\ell^{n,M}(z_k)}\right) \Psi_h(z_k)
\tag{24}
$$

being $\{z_k, w_k\}_{k=1}^K$ respectively the nodes and the weights. We remark that the local quantities in the Gaussian nodes are computed accordingly to (20) and the shift and scale method defined by (11) permits to preserve exactly mass, momentum and energy in each cell and at each collocation node.

Algorithm 3 sG BGK collision step.
- Compute the initial gPC expansions $\{x_i^{M,0}, v_i^{M,0}\}_{i=1}^N$ from the initial distribution $f^0(x, v)$;
- compute the velocities $\{\tilde{v}_i\}_{i=1}^N$ by sampling a standard normal distribution $\mathcal{N}(0, 1)$ according to (11);
- for $n = 0$ to $n_{\mathrm{TOT}} - 1$, given the projections $\{\hat{x}_{i,h}^n, \hat{v}_{i,h}^n, i = 1, \ldots, N, h = 0, \ldots, M\}$:
  - compute $\rho_\ell^{n,M}(z_k), U_\ell^{n,M}(z_k), T_\ell^{n,M}(z_k)$ in each cell I_ℓ, with $\ell = 1, \ldots, N_\ell, k = 1, \ldots, K$ according to (20);
  - for every particle $i = 1, \ldots, N$:
    * select ξ uniformly in $(0, 1)$;
    * compute the post interaction projections $\hat{v}_{i,h}^{n+1}$ according to (22);
- end for.

Stochastic Vlasov transport step. In the presence of uncertainties the equations of motion of the particles are given by

$$\frac{dx_i(t, \mathbf{z})}{dt} = v_i(t, \mathbf{z}), \qquad \frac{dv_i(t, \mathbf{z})}{dt} = E(x_i, t, \mathbf{z}).$$

The gPC expansion of the particles' systems $x_i^M(t, \mathbf{z}), v_i^M(t, \mathbf{z})$ is solution to

$$\frac{dx_i^M(t, \mathbf{z})}{dt} = v_i^M(t, \mathbf{z}), \qquad \frac{dv_i^M(t, \mathbf{z})}{dt} = E^M(x_i^M, t, \mathbf{z}).$$

Hence, we project the latter set of ODEs in the linear space $\{\Psi_h(\mathbf{z})\}_{h=0}^M$ to obtain

$$\frac{d\hat{x}_{i,h}(t)}{dt} = \hat{v}_{i,h}(t), \qquad \frac{d\hat{v}_{i,h}(t)}{dt} = \int_\Omega E^M(x_i^M, t, \mathbf{z})\Psi_h(\mathbf{z})p(\mathbf{z})d\mathbf{z}. \tag{25}$$

Considering the time and spatial discretization introduced before, given the projections $\{\hat{x}_{i,h}^n, \hat{v}_{i,h}^n\}$ and the electric field $\{E_\ell^{n+1/2,M}(\mathbf{z})\}_{\ell=1}^{N_\ell}$, the three step method at the level of projected quantities reads

$$\hat{x}_{i,h}^{n+1/2} = \hat{x}_{i,h}^n + \hat{v}_{i,h}^n \Delta t/2, \tag{26}$$

$$\hat{v}_{i,h}^{n+1} = \hat{v}_{i,h}^n + \Delta t \sum_{\ell=1}^{N_\ell} \int_\Omega E_\ell^{n+1/2,M}(\mathbf{z})\chi(x_i^{n+1/2,M}(\mathbf{z}) \in I_\ell)\Psi_h(\mathbf{z})p(\mathbf{z})d\mathbf{z}, \tag{27}$$

$$\hat{x}_{i,h}^{n+1} = \hat{x}_{i,h}^{n+1/2} + \hat{v}_{i,h}^{n+1}\Delta t/2. \tag{28}$$

The integral in (27) is again computed with Gauss quadrature on K nodes: as a consequence, the electric field needs to be calculated for every Gaussian nodes. This can be done by solving in parallel the Poisson equation as exposed in Section 3.1 for every $\{z_k\}_{k=1}^K$.

Since $m(\mathbf{z})$ does not depend on time and does not affect the dynamics, the scheme conserves the total mass. Moreover, the following proposition holds.

Proposition 1. *The sG Vlasov transport step conserves the total momentum provided the Poisson solver is such that*

$$\sum_{\ell=1}^{N_\ell} E_\ell^{n+1/2,M}(\mathbf{z})\rho_\ell^{n+1/2,M}(\mathbf{z}) = 0, \tag{29}$$

at each collocation node used to evaluate (27).

Proof. Summing up the contributions of all the particles we obtain from (27)

$$\sum_{i=1}^N \hat{v}_{i,h}^{n+1} = \sum_{i=1}^N \hat{v}_{i,h}^n + \Delta t \sum_{\ell=1}^{N_\ell} \int_\Omega E_\ell^{n+1/2,M}(\mathbf{z}) \sum_{i=1}^N \chi(x_i^{n+1/2,M}(\mathbf{z}) \in I_\ell)\Psi_h(\mathbf{z})p(\mathbf{z})d\mathbf{z}$$

$$= \sum_{i=1}^N \hat{v}_{i,h}^n + \Delta t \int_\Omega \frac{N}{m(\mathbf{z})}\left(\sum_{\ell=1}^{N_\ell} E_\ell^{n+1/2,M}(\mathbf{z})\rho_\ell^{n+1/2,M}(\mathbf{z})\right)\Psi_h(\mathbf{z})p(\mathbf{z})d\mathbf{z},$$

with $\rho_\ell^M(\mathbf{z})$ defined in (20). Now, since by assumption (29) the term within brackets vanishes at the collocation nodes used to evaluate the above integral, we have

$$\sum_{i=1}^{N} \hat{v}_{i,h}^{n+1} = \sum_{i=1}^{N} \hat{v}_{i,h}^{n}$$

which implies moment conservation. $\quad \square$

Algorithm 4 sG Vlasov transport step.

- Compute the initial gPC expansions $\{x_i^{0,M}, v_i^{0,M}\}_{i=1}^{N}$ from the initial distribution $f^0(x, v)$;
- for $n = 0$ to $n_{\text{TOT}} - 1$,
  given the projections $\{(\hat{x}_{i,h}^n, \hat{v}_{i,h}^n), i = 1, \dots, N, h = 0, \dots, M\}$:
  - compute the free transport on $\Delta t/2$ according to (26), and apply the boundary conditions;
  - compute the mass $\rho_l^{n+1/2}(z_k)$ in the nodes and then the electric field $\{E_l^{n+1/2}(z_k)\}_{l=1}^{N_l}$ by solving the Poisson equation with a mesh based method satisfying condition (29);
  - update the velocities on Δt according to (27)
  - compute the free transport on $\Delta t/2$ according to (28), and apply the boundary conditions;
- end for.

In the following we are interested both in periodic and reflecting boundary conditions on the space domain $I = [L_-, L_+]$ discretized by means of N_ℓ cells. To this end, we may observe that periodic conditions correspond to rewrite the position of the ith particle at time t^n as follows

$$x_i^{n,M}(\mathbf{z}) = \begin{cases} x_i^{n,M}(\mathbf{z}) & L_- \leq x_i^{n,M}(\mathbf{z}) \leq L_+ \\ x_i^{n,M}(\mathbf{z}) + (L_+ - L_+) & x_i^{n,M}(\mathbf{z}) < L_- \\ x_i^{n,M}(\mathbf{z}) - (L_+ - L_+) & x_i^{n,M}(\mathbf{z}) > L_+. \end{cases}$$

Therefore, at the level of projections we have for all $h = 0, \dots, M$

$$\hat{x}_{i,h}^n = \int_\Omega \left\{ \chi\left(x_i^{n,M}(\mathbf{z}) < L_-\right)\left(x_i^{n,M}(\mathbf{z}) + (L_+ - L_-)\right) + \chi\left(x_i^{n,M}(\mathbf{z}) > L_+\right)\left(x_i^{n,M}(\mathbf{z}) - (L_+ - L_-)\right) \right.$$

$$\left. + \chi\left(L_- \leq x_i^{n,M}(\mathbf{z}) \leq L_+\right) x_i^{n,M}(\mathbf{z}) \right\} \Psi_h(\mathbf{z}) p(\mathbf{z}) d\mathbf{z}. \tag{30}$$

On the other hand, reflecting boundary conditions [34] on the pair $(\tilde{x}_i^{n,M}(\mathbf{z}), \tilde{v}_i^{n,M}(\mathbf{z}))$ reads

$$\begin{cases} x_i^{n,M}(\mathbf{z}) = \tilde{x}_i^{n,M}(\mathbf{z}), \\ v_i^{n,M}(\mathbf{z}) = \tilde{v}_i^{n,M}(\mathbf{z}) & \text{if} \quad L_- \leq x_i^{n,M}(\mathbf{z}) \leq L_+ \\ x_i^{n,M}(\mathbf{z}) = L_- - |\tilde{x}_i^{n,M}(\mathbf{z}) + L_+|\text{sgn}(\tilde{v}_i^{n,M}(\mathbf{z})), \\ v_i^{n,M}(\mathbf{z}) = -\tilde{v}_i^{n,M}(\mathbf{z}) & \text{if} \quad x_i^{n,M}(\mathbf{z}) < L_- \\ x_i^{n,M}(\mathbf{z}) = L_+ - |\tilde{x}_i^{n,M}(\mathbf{z})L_-|\text{sgn}(\tilde{v}_i^{n,M}(\mathbf{z})), \\ v_i^{n,M}(\mathbf{z}) = -\tilde{v}_i^{n,M}(\mathbf{z}) & \text{if} \quad x_i^{n,M}(\mathbf{z}) > L_+, \end{cases}$$

from which we have the projections for all $h = 0, \dots, M$

$$\hat{x}_{i,h}^n = \int_\Omega \left\{ \chi\left(\tilde{x}_i^{n,M}(\mathbf{z}) < L_-\right)\left(L_- - |\tilde{x}_i^{n,M}(\mathbf{z}) + L_+|\text{sgn}(\tilde{v}_i^{n,M}(\mathbf{z}))\right) \right.$$

$$+ \chi\left(\tilde{x}_i^{n,M}(\mathbf{z}) > L_+\right)\left(L_+ - |\tilde{x}_i^{n,M}(\mathbf{z})L_-|\text{sgn}(\tilde{v}_i^{n,M}(\mathbf{z}))\right) \tag{31}$$

$$\left. + \chi\left(L_- \leq \tilde{x}_i^{n,M}(\mathbf{z}) \leq L_+\right)\tilde{x}_i^{n,M}(\mathbf{z}) \right\} \Psi_h(\mathbf{z}) p(\mathbf{z}) d\mathbf{z},$$
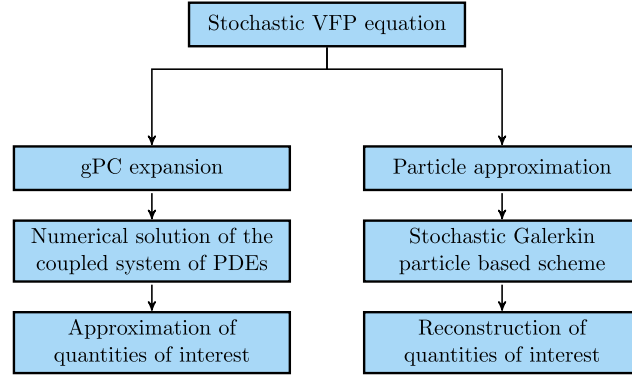
Fig. 1. Numerical approaches to stochastic Vlasov-Fokker-Planck equations. The left branch describes the classical sG approach based on finite differences/volumes, whereas the right branch sketches the stochastic particle Galerkin approach.

$$
\hat{v}_{i,h}^n = \int_{\Omega} \left\{ \chi \left(\tilde{x}_i^{n,M}(\mathbf{z}) < L_- \right) \left(-\tilde{v}_i^{n,M} \right) + \chi \left(\tilde{x}_i^{n,M}(\mathbf{z}) > L_+ \right) \left(-\tilde{v}_i^{n,M} \right) \right.
$$

$$
\left. + \chi \left(L_- \leq \tilde{x}_i^{n,M}(\mathbf{z}) \leq L_+ \right) \tilde{v}_i^{n,M}(\mathbf{z}) \right\} \Psi_h(\mathbf{z}) p(\mathbf{z}) d\mathbf{z}.
\tag{32}
$$

As before, the integrals are computed with Gaussian quadrature.

Approximation of quantities of interest. To analyze the effects of uncertainties on the kinetic model (1) we are generally interested in quantities of interest (QoI) $q[f]$ that can be computed from the distribution function. In the present setting, the QoI is simply the identity, i.e. $q[f] = f$. Anyway, more generally, it may be given by any moment of the kinetic solution.

In Fig. 1 we sketch two approaches for the approximation of QoI of the Vlasov-Fokker-Planck equation. In the left branch we find the standard sG approach, in which we first consider the gPC approximation of the original problem that generates a coupled system of VFP-type PDEs. The resulting systems can be solved by classical deterministic finite difference/volume methods. In the right branch we describe instead the stochastic Galerkin particle reformulation of the problem, in which the gPC approximation is considered at the particle level. We highlight that, in view of the above particle reformulation of the problem, the distribution is defined from a sample of N particles $\{x_i^n(\mathbf{z}), v_i^n(\mathbf{z})\}_{i=1}^N$ as follows

$$
f_N^n(x, v, \mathbf{z}) = \frac{m(\mathbf{z})}{N} \sum_{i=1}^N \delta(x - x_i^n(\mathbf{z})) \otimes \delta(v - v_i^n(\mathbf{z})),
$$

where $\delta(\cdot)$ is the Dirac delta. In particular, we approximate this quantity as

$$
f_N^{n,M}(x, v, \mathbf{z}) = \frac{m(\mathbf{z})}{N} \sum_{i=1}^N \delta(x - x_i^{n,M}(\mathbf{z})) \otimes \delta(v - v_i^{n,M}(\mathbf{z})),
$$

having defined $\{x_i^{n,M}(\mathbf{z}), v_i^{n,M}(\mathbf{z})\}_{i=1}^N$ in (17) and where $(\hat{x}_{i,h}^n, \hat{v}_{i,h}^n)$ are solution of (22) for the collision step and of (26)-(27)-(28) for the transport step.

4. Numerical tests

In this section, we present several numerical results for the DSMC-sG Algorithm 3 and 4. In all the following tests, we consider the second order Strang splitting method exposed in Section 3 on the time interval $[0, t_f]$. We restrict to bidimensional phase space $(x, v) \in \mathbb{R} \times \mathbb{R}$, for the sake of simplicity, however the results hold also in higher-dimensional phase space. We reconstruct the densities through histograms with $N_\ell = 100$ cells in the spatial domain and $N_v = 200$ cells in the velocity domain. The Poisson equation is solved with a finite difference method on a uniform grid of $N_x = N_\ell + 1 = 101$ points, with periodic or Dirichlet boundary conditions [45], adopting a stochastic collocation approach [49]. In all the test we considered uniform uncertainties, that are linked to Legendre polynomials in the Wiener-Askey scheme, see [50]. The details of the initial sampling techniques are presented in Appendix A.

First we consider the linear and nonlinear Landau damping, then we check the spectral convergence of the scheme and we investigate another standard plasma test, the two stream instability, both in linear and nonlinear case. In the end, we investigate the hydrodynamic limit of the model with the standard Sod shock tube test.

4.1. Test 1: Landau damping

The Landau damping [29,47] in one of the greatest theoretical results of the collisionless plasma physics. It corresponds to the exponential decay of the electromagnetic waves without energy dissipation, as a result of the wave-particle interaction. The charged particles in motion with a velocity lower than the phase velocity of the wave gain energy from it, leading to the electromagnetic energy damping. On the contrary, particles with a velocity greater than the phase velocity yield energy to the wave, causing its energy increasing. As a result, although the total energy of the Vlasov-Poisson equation is conserved for every $\mathbf{z} \in \mathbb{R}^{d_z}$, i.e.

$$\frac{d}{dt}\left[\frac{1}{2}\int\limits_{\mathbb{R}^3}\int\limits_{\mathbb{R}^3} |v|^2 f(x,v,t,\mathbf{z})dxdv + \frac{1}{2}\int\limits_{\mathbb{R}^3}|E(x,t,\mathbf{z})|^2dx\right] = 0,$$

if there are more particles with $v < v_\phi$ than particles with $v > v_\phi$, we may observe the decay of the L^2-norm of the electric field

$$\mathcal{E}(t,\mathbf{z}) = \left(\int\limits_{\mathbb{R}^3}|E(x,t,\mathbf{z})|^2dx\right)^{\frac{1}{2}} \tag{33}$$

with a specific damping rate γ. If we consider also a small but finite collision frequency ν, the damping is balanced by the interactions among the particles and, in the limit $\nu \to +\infty$, we recover the fluid limit of the Vlasov equation with the electric field fluctuating around a constant value.

To observe the Landau damping, we consider a wave perturbation of the local Maxwellian distribution. If the perturbation is small, we are in the so-called *linear Landau damping* regime, if the wave amplitude increases, we get the *nonlinear Landau damping* regime.

Linear case. We consider, at the initial time, an uncertain perturbation of the local equilibrium

$$f_0(x,v,\mathbf{z}) = (1 + \alpha(\mathbf{z})\cos(kx))\frac{1}{\sqrt{2\pi T}}e^{-\frac{v^2}{2T}}, \tag{34}$$

with $x \in [0, 2\pi/k]$, k wave number and $\alpha(\mathbf{z})$ small random amplitude. The temperature is fixed $T = 1$.

To observe the phenomenon, the velocity domain has to be larger than the phase velocity of the wave $v_\phi = \omega/k$, where ω is the frequency and v_ϕ is the singularity of the dispersion relation. According to [13], the frequency ω can be estimated as

$$\omega^2 = 1 + 3k^2,$$

while, for small wave numbers, a more accurate formula [31] gives

$$\omega^2 = 1 + 3k^2 + 6k^4 + 12k^6.$$

In the collisionless regime [10], we are able to provide an approximation also for the damping rate γ, that is

$$\gamma = -\sqrt{\frac{\pi}{8}}\frac{1}{k^3}\exp\left(-\frac{1}{2k^2} - \frac{3}{2}\right)$$

for large k, and

$$\gamma = -\sqrt{\frac{\pi}{8}}\left(\frac{1}{k^3} - 6k\right)\exp\left(-\frac{1}{2k^2} - \frac{3}{2} - 3k^2 - 12k^4\right)$$

for smaller wave number.

We consider $N = 10^7$ particles, $\Delta t = 0.1$, $M = 5$ for the stochastic Galerkin projection and $\alpha(\mathbf{z}) = \frac{1}{20} + \frac{1}{10}\mathbf{z}$, $\mathbf{z} \sim \mathcal{U}([0,1])$ in (34). We select $k = 0.5$ and we investigate different collisional regimes corresponding to the choices $\nu = 0, 1, 10^3$. We apply periodic boundary conditions on the particles in the space domain according to (30) and on the Poisson equation.

In Fig. 2 we show the logarithm of the expectation and the variance of $\mathcal{E}(t,\mathbf{z})$. As expected, in the collisionless scenario $\nu = 0$, the numerical results are in agreement with the theoretical damping rate $\gamma = -0.1533$ and with the approximation of the electric field obtained, e.g., in [45]. With a collision frequency $\nu = 1$, we observe that the interactions between the particle balance the damping and the electric field exhibits a slower decreasing with respect to the collisionless case. With a bigger frequency $\nu = 10^3$, we note that the electric field fluctuates around a constant value, as expected (see, e.g., [17]).
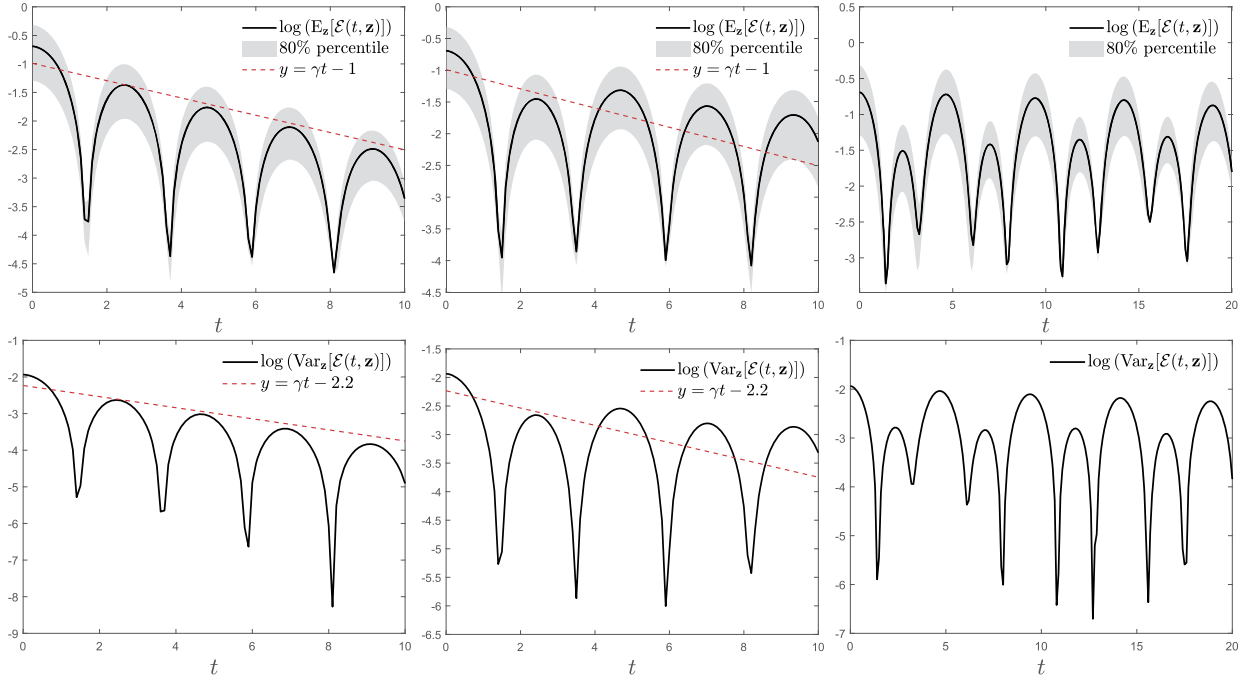
Fig. 2. Test 1: linear Landau damping. Logarithm of $\mathbb{E}_\mathbf{z}[\mathcal{E}(t, \mathbf{z})]$ (top row) and $\mathrm{Var}_\mathbf{z}[\mathcal{E}(t, \mathbf{z})]$ (bottom row) for $\nu = 0$ (left), $\nu = 1$ (centre) and $\nu = 10^3$ (right) in linear Landau damping. We choose $k = 0.5$, $N = 10^7$ particles, $M = 5$ and $\Delta t = 0.1$. We considered the initial condition (34) with $\alpha(\mathbf{z}) = \frac{1}{20} + \frac{1}{10}\mathbf{z}$, $\mathbf{z} \sim \mathcal{U}([0, 1])$. The theoretical damping rate is $\gamma = -0.1533$.

As we can observe from the bottom row of Fig. 2, the dynamics of the variance shows a time evolution that is similar to the expected value. This is an effect of the linear perturbation regime, since the oscillation frequency of the electromagnetic wave depends only on the wave number.

Nonlinear case. We investigate now the nonlinear case, that is, we consider the initial distribution (34) with $N = 5 \cdot 10^7$ particles and the same computational setting as before with the only difference of a greater perturbation amplitude. In particular, we choose $\alpha(\mathbf{z}) = \frac{2}{5} + \frac{3}{5}\mathbf{z}$, $\mathbf{z} \sim \mathcal{U}([0, 1])$, in the collisionless scenario $\nu = 0$, and $\alpha(\mathbf{z}) = \frac{1}{5} + \frac{2}{5}\mathbf{z}$, $\mathbf{z} \sim \mathcal{U}([0, 1])$, for $\nu = 1, 10^3$.

The analytical estimations obtained in the previous paragraph via the linear theory no longer hold. Since the electric potential is larger, it could happen that particles remain trapped in the potential well of the electromagnetic wave. This is the so-called *electron trapping*. The trapped particles, fluctuating into the well, cause both damping and growth of the electric field. In literature there exist several approximations for the damping γ_d and growth γ_g rates in the nonlinear regime, from which we can compare our numerical results, see e.g. [4,9,17,24,30,41] and the references therein.

As we can observe in Fig. 3, in the collisionless scenario the numerical results are in accordance with the theoretical approximations of the rates, i.e. $\gamma_d = -0.2920$ and $\gamma_g = 0.0815$. With collision frequencies $\nu = 1, 10^3$, we observe that the interactions between the particles induce slight different behaviors of the electric energy, balancing the damping and growth behavior. We observe also that the variance, as the time increases, exhibits a shift in the peaks of oscillation. Unlike the linear case, the frequency of the electric wave appears as dependent on the initial uncertain amplitude.

In Fig. 4 we show the typical profiles of the expectation and variance of the distributions in the collisionless case, at fixed times $t = 10, 30, 50$ and we note that the expected value and the variance in $\mathbf{z}$ exhibit similar foliation patterns.

4.2. Test 2: spectral convergence

We numerically check for the convergence in the space of the random parameters of the Algorithm 4, i.e. the collisionless Vlasov-Poisson system with $\nu = 0$.

We consider the initial distribution

$$f_0(x, v, \mathbf{z}) = \rho(x) \frac{1}{\sqrt{2\pi T(\mathbf{z})}} e^{-\frac{v^2}{2T(\mathbf{z})}}, \tag{35}$$

with initial random temperature $T(\mathbf{z}) = \frac{4}{5} + \frac{2}{5}\mathbf{z}$, $\mathbf{z} \sim \mathcal{U}([0, 1])$ and mass

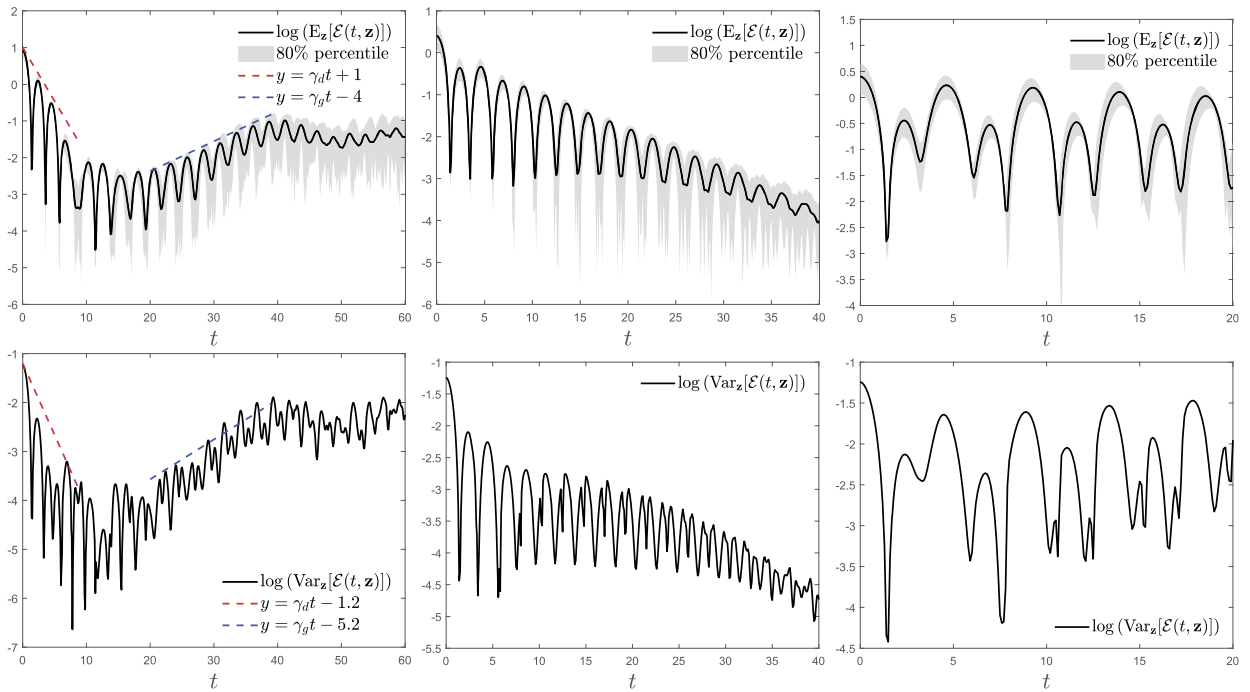$$\rho(x) = \frac{1}{\sqrt{\pi}} e^{-(x-6)^2}$$

Fig. 3. Test 1: nonlinear Landau damping. Logarithm of $\mathbb{E}_{\mathbf{z}}[\mathcal{E}(t, \mathbf{z})]$ (top row) and $\mathrm{Var}_{\mathbf{z}}[\mathcal{E}(t, \mathbf{z})]$ (bottom row) for $\nu = 0$ (left), $\nu = 1$ (centre) and $\nu = 10^3$ (right) in nonlinear Landau damping. We choose $k = 0.5$, $N = 5 \cdot 10^7$ particles, $M = 5$ and $\Delta t = 0.1$. We considered the initial condition (34) with $\alpha(\mathbf{z}) = \frac{2}{5} + \frac{3}{5}\mathbf{z}$, $\mathbf{z} \sim \mathcal{U}([0, 1])$. In the collisionless scenario the damping rate is $\gamma_d = -0.2920$ and the growth rate is $\gamma_g = 0.0815$.
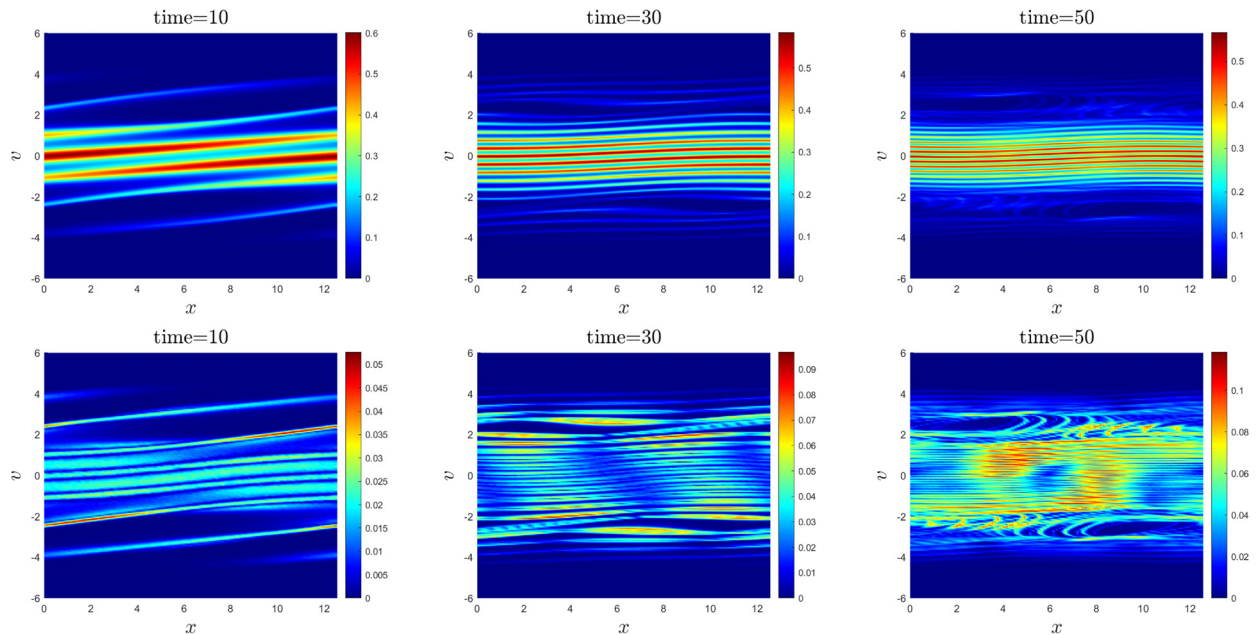
Fig. 4. Test 1: nonlinear Landau damping. We report $\mathbb{E}_{\mathbf{z}}[f(x, v, t, \mathbf{z})]$ (top row) and $\mathrm{Var}_{\mathbf{z}}[f(x, v, t, \mathbf{z})]$ (bottom row) at fixed times $t = 10, 30, 50$, in collisionless nonlinear Landau damping. We choose $k = 0.5$, $N = 5 \cdot 10^7$ particles, $M = 5$ and $\Delta t = 0.1$. We considered the initial condition (34) with $\alpha(\mathbf{z}) = \frac{2}{5} + \frac{3}{5}\mathbf{z}$, $\mathbf{z} \sim \mathcal{U}([0, 1])$.

in the physical domain $x \in [0, 4\pi]$. We use $N = 10^6$ particles and $\Delta t = 0.1$, solving the Poisson equation with periodic boundary conditions.

To observe the convergence, we consider a reference sG particle solution obtained with $M = 30$ and we store the initial data, the only source of randomness of the scheme, so that the same data is used for the different values of M. In Fig. 5 we show in semilogarithmic scale the decay of the L^2 error in the evaluation of the observable $\mathcal{E}(t, \mathbf{z})$ defined in (33), for
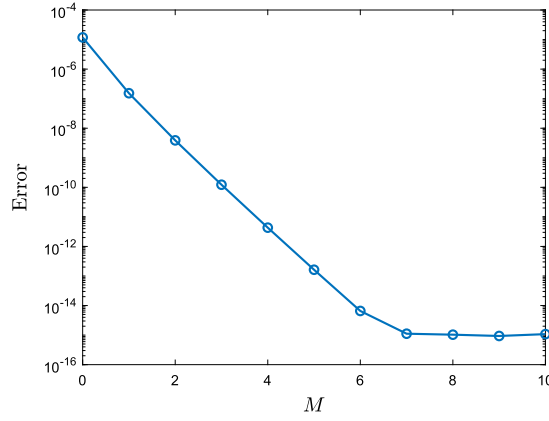
Fig. 5. Test 2: spectral convergence. L^2 error in the evaluation of $\mathcal{E}(t, \mathbf{z})$ of the sG particle scheme at fixed time $t = 1$. We consider $N = 10^6$ particles, $\Delta t = 0.1$ and a reference solution computed with $M = 30$. We consider the initial condition (35) with $T(\mathbf{z}) = \frac{4}{5} + \frac{2}{5}\mathbf{z}$, $\mathbf{z} \sim \mathcal{U}([0, 1])$.
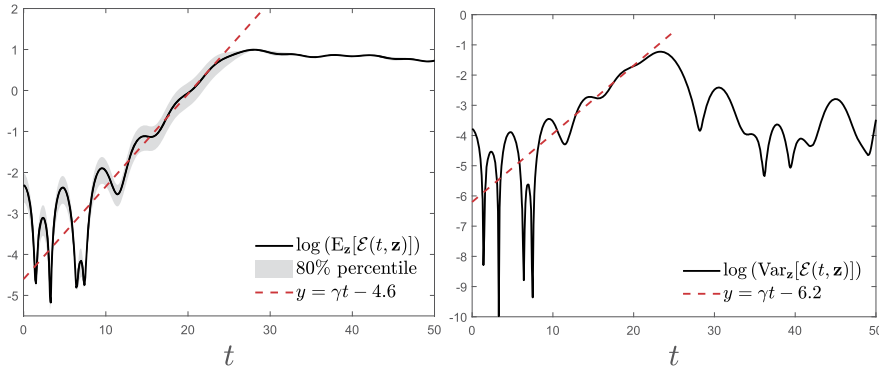

Fig. 6. Test 3: linear two stream instability. Logarithm of $\mathbb{E}_\mathbf{z}[\mathcal{E}(t, \mathbf{z})]$ (left) and $\text{Var}_\mathbf{z}[\mathcal{E}(t, \mathbf{z})]$ (right) in collisionless linear two stream instability. We choose $k = 0.2$, $N = 5 \cdot 10^7$ particles, $M = 5$ and $\Delta t = 0.1$. We considered the initial condition (36) with $\alpha(\mathbf{z}) = 3 \cdot 10^{-3} + 4 \cdot 10^{-3}\mathbf{z}$, $\mathbf{z} \sim \mathcal{U}([0, 1])$. The theoretical growth rate is $\gamma = 0.2258$.

increasing M and at fixed time $t = 1$. Exponential decay of the error up to machine precision is observed, which shows that the sG particle scheme is spectrally accurate in the space of the random parameters.

4.3. Test 3: two stream instability

Another classical effect of the collisionless plasma is the so-called two stream instability. If we initialize the electron velocities as a non-isotropic two beam distribution, contrary to the Landau damping, we have more particles with $v > v_\phi$ than particles with $v < v_\phi$. As a consequence, the electromagnetic wave gains energy from the electrons, giving birth to instabilities represented by typical swirling and warped pattern of the particle distribution function. In the following, we will investigate the linear and the nonlinear case.

Linear case. We consider the initial distribution

$$f_0(x, v, \mathbf{z}) = (1 + \alpha(\mathbf{z})\cos(kx))\frac{1}{\sqrt{2\pi T}}\left(e^{-\frac{(v - \bar{v})^2}{2T}} + e^{-\frac{(v + \bar{v})^2}{2T}}\right), \tag{36}$$

with fixed temperature $T = 1$ and $\bar{v} = 2.4$. As before, we have $x \in [0, 2\pi/k]$.

In the collisionless scenario, if the perturbation amplitude is small enough, after a certain amount of time the logarithm of the L^2-norm of the electric energy grows linearly with a specific rate γ, see e.g. [10,30,48].

We choose $N = 5 \cdot 10^7$ particles $M = 5$, $k = 0.2$, $v = 0$ and $\alpha(\mathbf{z}) = 3 \cdot 10^{-3} + 4 \cdot 10^{-3}\mathbf{z}$, $\mathbf{z} \sim \mathcal{U}([0, 1])$. As in the Landau damping tests, we apply periodic boundary conditions on the particles and on the Poisson equation. In Fig. 6, we show the expectation and variance of the electric energy and we observe that the results fit the theoretical linear growth of $\gamma = 0.2258$. After a certain point, we note that the mean reaches a stable value with a non zero variance, meaning that the uncertainties are not dampened by the dynamics of the model.

In Fig. 7, we present the expectations and variances of the distribution at fixed times $t = 0, 20, 50$. As the time increases, the typical whirling profiles of the linear two stream instability become more evident both in the mean and the variance.
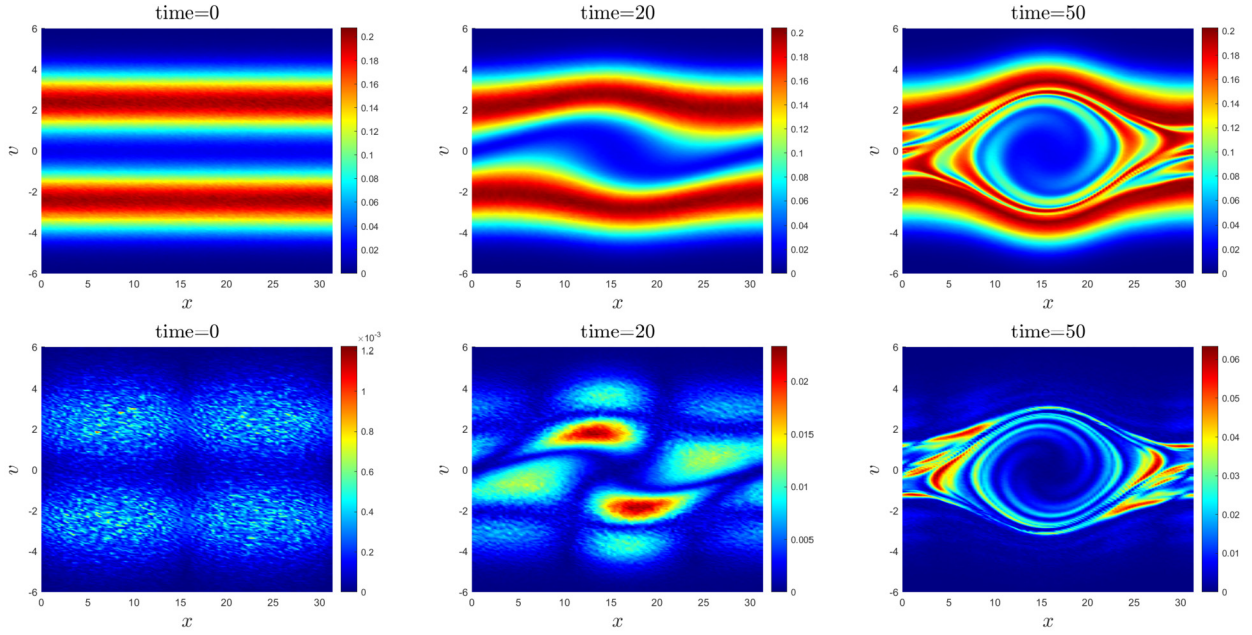
Fig. 7. Test 3: linear two stream instability. We report $\mathbb{E}_{\mathbf{z}}[f(x,v,t,\mathbf{z})]$ (top row) and $\text{Var}_{\mathbf{z}}[f(x,v,t,\mathbf{z})]$ (bottom row) at fixed times $t=0,20,50$, in collisionless linear two stream instability. We choose $k=0.2$, $N=5\cdot10^7$ particles, $M=5$ and $\Delta t=0.1$. We considered the initial condition (36) with $\alpha(\mathbf{z})=3\cdot10^{-3}+4\cdot10^{-3}\mathbf{z}$, $\mathbf{z}\sim\mathcal{U}([0,1])$.

Nonlinear case. We consider here the nonlinear two stream instability. We choose the initial conditions

$$f_0(x,v,\mathbf{z})=(1+\alpha(\mathbf{z})\cos(kx))\frac{1}{\sqrt{2\pi T}}\left(e^{-\frac{(v-\bar{v})^2}{2T}}+e^{-\frac{(v+\bar{v})^2}{2T}}\right),\tag{37}$$

with fixed temperature $T=0.3$, $\bar{v}=0.99$ and wave number $k=2/13$. The physical domain is $x\in[0,2\pi/k]$. We apply periodic boundary conditions on the particles and on the Poisson equation.

We choose $N=5\cdot10^7$ particles, $M=5$, $\Delta t=0.1$ and the perturbation amplitude $\alpha(\mathbf{z})=4\cdot10^{-2}+2\cdot10^{-2}\mathbf{z}$, $\mathbf{z}\sim\mathcal{U}([0,1])$. In the following, we investigate different collisional regimes corresponding to the choices $\nu=0,1,10^3$.

In the collisionless scenario, the nonlinear phenomenon of the electron trapping causes stronger distortions of the distribution $f(x,v,t,\mathbf{z})$, which can not be treated analytically, as we can observe from $\mathbb{E}_{\mathbf{z}}[f(x,v,t,\mathbf{z})]$ in Fig. 8 at times $t=0,15,20$. In the same figure we report the values of $\text{Var}_{\mathbf{z}}[f(x,v,t,\mathbf{z})]$ computed at the same times from which we get information on the deviation from expected trends.

If we consider a non-zero collision frequency ν, the interactions among the particles balance the electron trapping phenomenon letting the system reach the Maxwellian equilibrium quickly, as we can see from Fig. 9 and 10.

4.4. Test 4: Sod shock tube

To evaluate the capability of the sG particle scheme to capture the limit Euler-Poisson system (5), we perform the Sod shock tube test [44] for different collisional regimes, comparing our results with a collocation method applied to a Lax-Fridrichs and a WENO scheme [42]. The test is a typical Riemann problem, namely it consists in a piecewise constant initial value problem with a discontinuity in the space domain. In particular, we consider two different settings: the first with an uncertain initial temperature, the second with an uncertain position of the interface.

Uncertain initial temperature. We consider the initial distribution

$$f_0(x,v,\mathbf{z})=\frac{\rho_0(x)}{\sqrt{2\pi T_0(x,\mathbf{z})}}e^{-\frac{v^2}{2T_0(x,\mathbf{z})}},$$

with $x\in[0,1]$. The mass $\rho_0(x)$ and the uncertain temperature $T_0(x,\mathbf{z})$ are initialized as

$$\begin{aligned}\rho_0(x)=1,\quad&T_0(x,\mathbf{z})=1+\alpha(\mathbf{z})&\text{if }0<x<0.5\\\rho_0(x)=0.125,\quad&T_0(x,\mathbf{z})=0.8+\alpha(\mathbf{z})&\text{if }0.5<x<1\end{aligned}\tag{38}$$
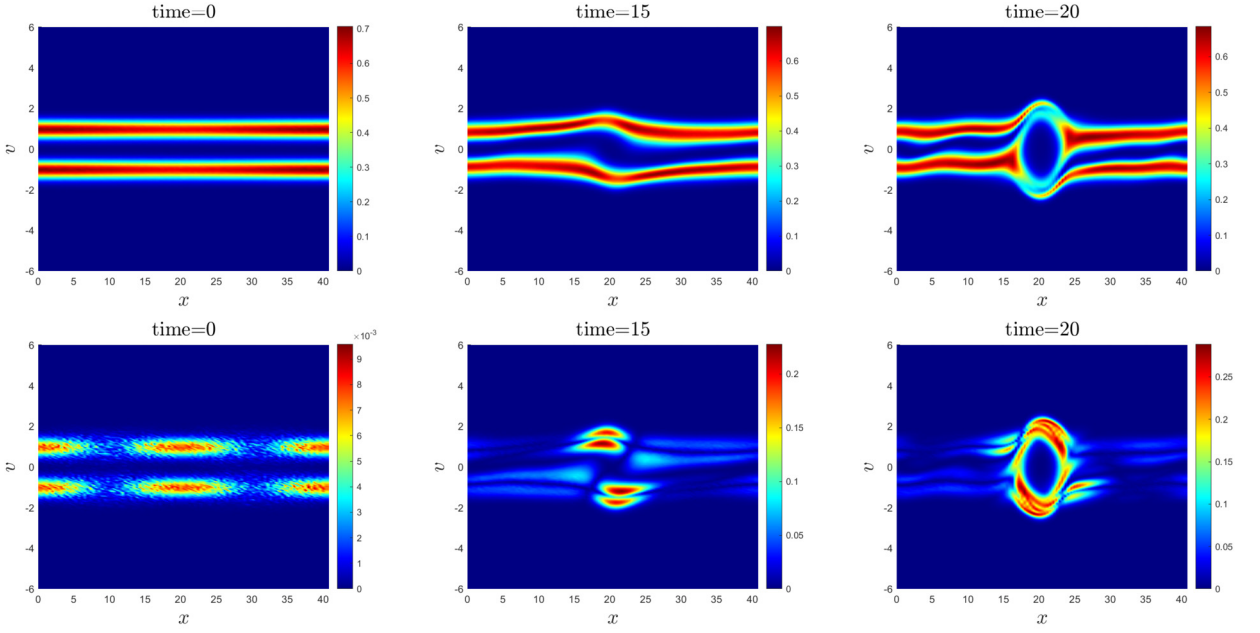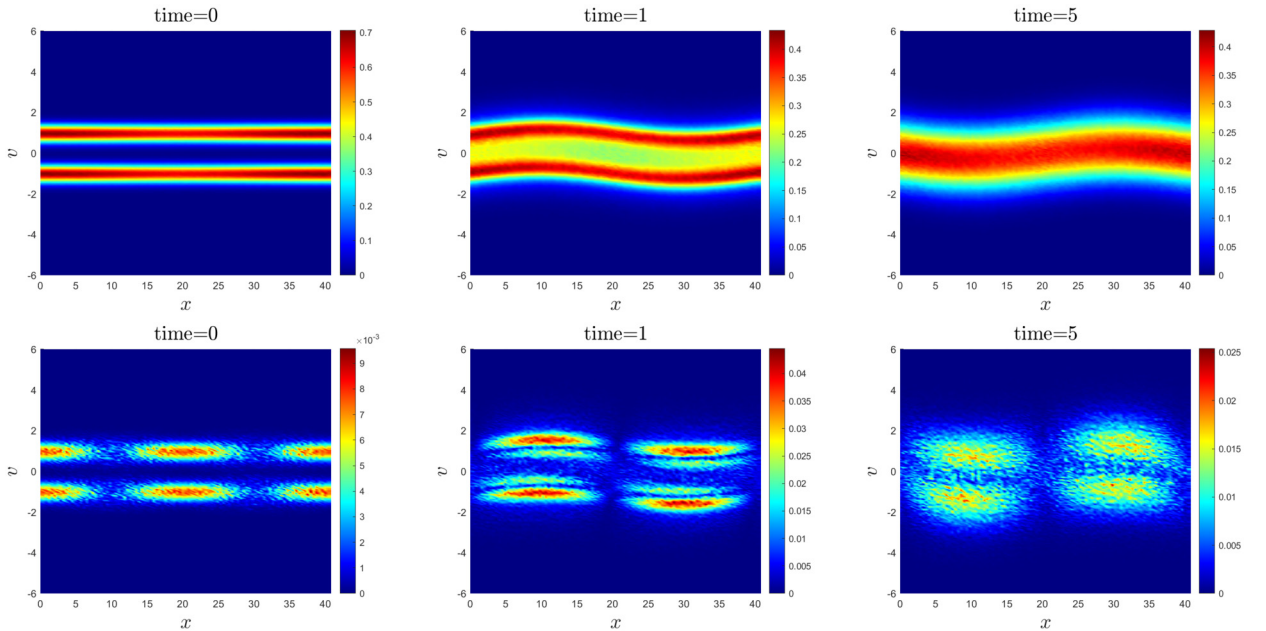
Fig. 8. Test 3: nonlinear two stream instability. We report $\mathbb{E}_{\mathbf{z}}[f(x, v, t, \mathbf{z})]$ (top row) and $\text{Var}_{\mathbf{z}}[f(x, v, t, \mathbf{z})]$ (bottom row) at fixed times $t = 0, 15, 20$, in collisionless nonlinear two stream instability. We choose $k = 2/13$, $N = 5 \cdot 10^7$ particles, $M = 5$ and $\Delta t = 0.1$. We considered the initial condition (37) with $\alpha(\mathbf{z}) = 4 \cdot 10^{-2} + 2 \cdot 10^{-2} \mathbf{z}$, $\mathbf{z} \sim \mathcal{U}([0, 1])$.

Fig. 9. Test 3: nonlinear two stream instability. We report $\mathbb{E}_{\mathbf{z}}[f(x, v, t, \mathbf{z})]$ (top row) and $\text{Var}_{\mathbf{z}}[f(x, v, t, \mathbf{z})]$ (bottom row) at fixed times $t = 0, 1, 5$, in nonlinear two stream instability with $\nu = 1$. We choose $k = 2/13$, $N = 5 \cdot 10^7$ particles, $M = 5$ and $\Delta t = 0.1$. We considered the initial condition (37) with $\alpha(\mathbf{z}) = 4 \cdot 10^{-2} + 2 \cdot 10^{-2} \mathbf{z}$, $\mathbf{z} \sim \mathcal{U}([0, 1])$.

with $\alpha(\mathbf{z}) = 0.25\mathbf{z}$, $\mathbf{z} \sim \mathcal{U}([0, 1])$. We choose $N = 10^7$, $M = 5$, $\Delta t = 0.01$ and we consider different collisional regimes corresponding to the choices $\nu = 1, 10^3$. We implement Dirichelet boundary conditions for the Poisson equation and reflecting boundary conditions for the particles according to (31) and (32).

We compute a reference solution with $N = 10^8$ particles, $N_\ell = 200$ cells, $\nu = 10^4$ and the other parameters as before, to compare the results of the two collisional regimes. In particular, we compare the expectations of the mass $\rho(x, \mathbf{z})$ and temperature $T(x, \mathbf{z})$ at the final time $t = 0.15$, with respect to the reference solution. In Fig. 11 we observe that for $\nu = 10^3$
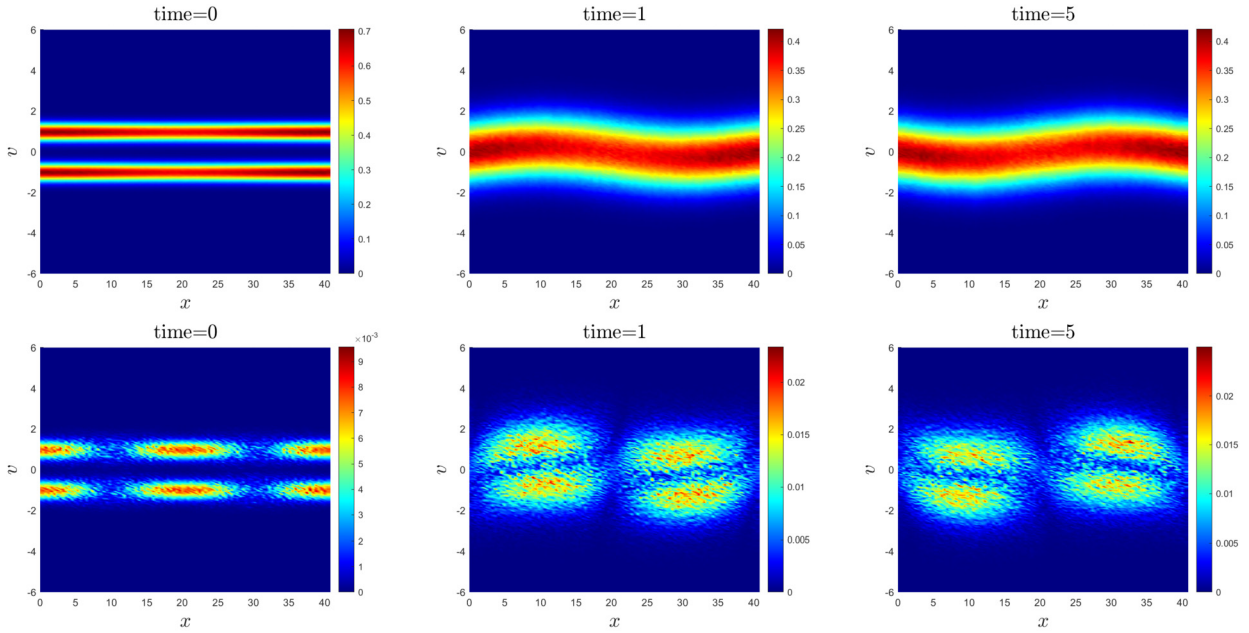
Fig. 10. Test 3: nonlinear two stream instability. We report $\mathbb{E}_{\mathbf{z}}[f(x, v, t, \mathbf{z})]$ (top row) and $\mathrm{Var}_{\mathbf{z}}[f(x, v, t, \mathbf{z})]$ (bottom row) at fixed times $t = 0, 1, 5$, in nonlinear two stream instability with $\nu = 10^3$. We choose $k = 2/13$, $N = 5 \cdot 10^7$ particles, $M = 5$ and $\Delta t = 0.1$. We considered the initial condition (37) with $\alpha(\mathbf{z}) = 4 \cdot 10^{-2} + 2 \cdot 10^{-2}\mathbf{z}$, $\mathbf{z} \sim \mathcal{U}([0, 1])$.

(top row) the mean values together with the confidence intervals fit the reference solution, while for $\nu = 1$ (bottom row) the frequency of collisions is obviously not enough to justify the fluid limit.

We solve the same uncertain Riemann problem with a first order in time and space Lax-Friedrichs (LF) method, and a third order in time, fifth order in space WENO scheme. For the uncertain parameter, we adopted a stochastic collocation method with 11 collocation nodes, LF is solved with 1500 cells and a CFL number equal to 0.1, WENO35 with 200 cells and CFL number 0.5. The results are summarized in Fig. 12. We observe that the reference particle sG solution (red circles) is in good accordance with the Lax-Friedrichs results (solid black line), since they both are first order.

Uncertain interface position. We consider now the distribution at the initial time

$$f_0(x, v, \mathbf{z}) = \frac{\rho_0(x, \mathbf{z})}{\sqrt{2\pi T_0(x, \mathbf{z})}} e^{-\frac{v^2}{2T_0(x, \mathbf{z})}},$$

with $x \in [0, 1]$. In this scenario, we design an uncertain initial interface, i.e.

$$\begin{aligned} \rho_0(x, \mathbf{z}) = 1, \qquad T_0(x, \mathbf{z}) = 1 \quad &\text{if} \quad 0 < x < 0.5 + \alpha(\mathbf{z}) \\ \rho_0(x, \mathbf{z}) = 0.125, \qquad T_0(x, \mathbf{z}) = 0.8 \quad &\text{if} \quad 0.5 + \alpha(\mathbf{z}) < x < 1 \end{aligned} \qquad (39)$$

with $\alpha(\mathbf{z}) = -0.05 + 0.1\mathbf{z}$, $\mathbf{z} \sim \mathcal{U}([0, 1])$. Again, we choose $N = 10^7$, $M = 5$, $\Delta t = 0.01$ and we consider different collisional regimes corresponding to the choices $\nu = 1, 10^3$. The boundary conditions for the particles and the Poisson equation are the same as the previous test.

The reference solution is computed with $N = 10^8$ particles, $N_\ell = 200$ cells, $\nu = 10^4$ and the other parameters as before. In Fig. 13 we show the expectations and the confidence intervals of the mass and temperature at the final time $t = 0.15$. We observe that in the collisional regime, assumed here to be characterized by the frequency $\nu = 10^3$ (top row), the results are in agreement with the reference solution. For $\nu = 1$ (bottom row) clearly the collision frequency is far from the fluid limit and the profiles computed from the kinetic density differ from the ones of reference solution.

As in the previous case, we compare the particle sG solver with a first order in time and space Lax-Friedrichs (LF) method, and a third order in time, fifth order in space WENO scheme. The computational setting is the same as before: we adopted a stochastic collocation method with 11 collocation nodes, LF is solved with 1500 cells and a CFL number equal to 0.1, WENO35 with 200 cells and CFL number 0.5. In Fig. 14 we may observe that the reference particle sG solution (red circles) is in good accordance with the Lax-Friedrichs results (solid black line).
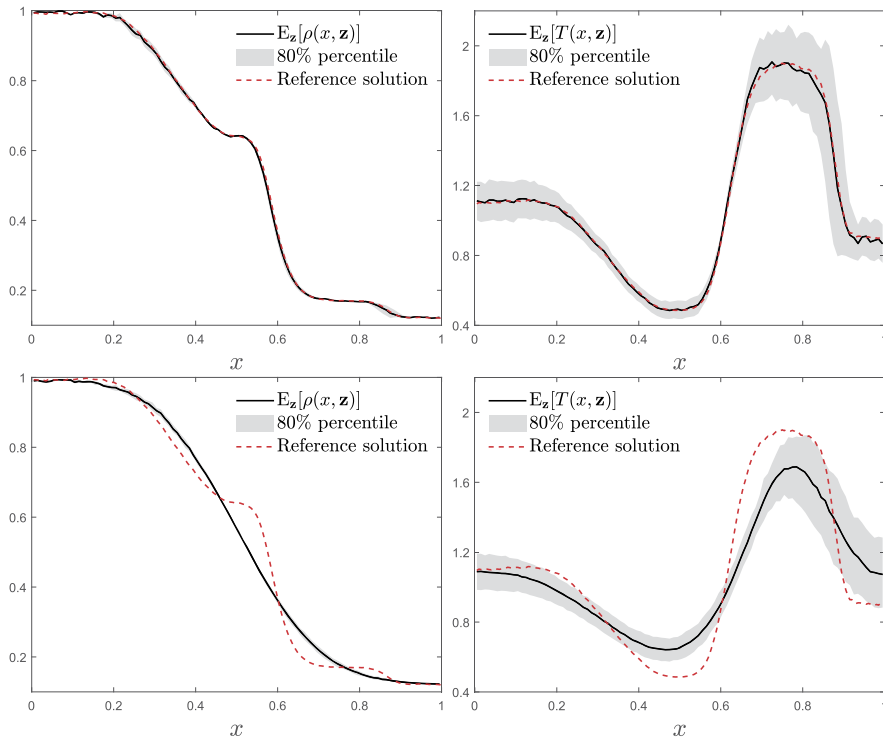
Fig. 11. Test 4: Sod shock tube. We report $\mathbb{E}_{\mathbf{z}}[\rho(x, t, \mathbf{z})]$ (left) and $\mathbb{E}_{\mathbf{z}}[T(x, t, \mathbf{z})]$ (right) for $\nu = 10^3$ (top) and $\nu = 1$ (bottom), at fixed times $t = 0.15$, for the Sod shock test with uncertain initial temperature. We choose $N = 10^7$, $M = 5$, $\Delta t = 0.01$. We considered the initial condition (38) with $\alpha(\mathbf{z}) = 0.25\mathbf{z}$, $\mathbf{z} \sim \mathcal{U}([0, 1])$. Reference solution computed with $N = 10^8$ particles.
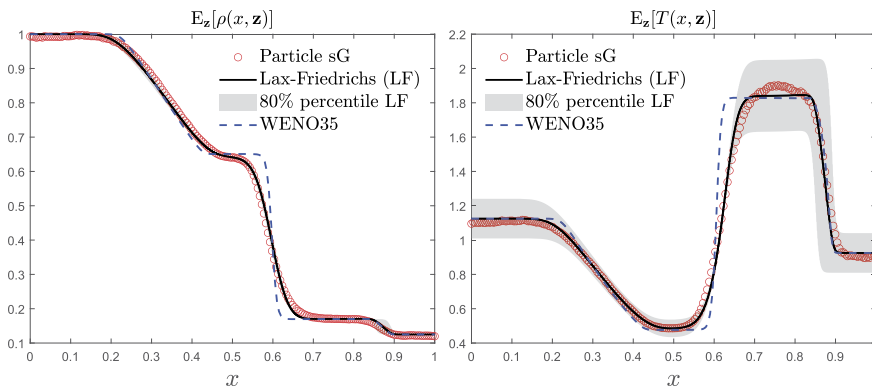
Fig. 12. Test 4: Sod shock tube. Comparison of the particle sG reference solution with Lax-Friedrichs and WENO schemes. We considered the initial condition (38) with $\alpha(\mathbf{z}) = 0.25\mathbf{z}$, $\mathbf{z} \sim \mathcal{U}([0, 1])$. The particle solution is computed with $N = 10^8$, $M = 5$ and $\Delta t = 0.01$. Lax-Friedrichs is solved with 1500 cells and CFL number 0.1, WENO with 200 cells and CFL number 0.5. In both cases we use a stochastic collocation approach with 11 nodes. (For interpretation of the colors in the figure(s), the reader is referred to the web version of this article.)

5. Conclusions

We presented a novel numerical method based on a sG projection of the corresponding particle dynamics for uncertainty quantification in collisional plasma physics. From a mathematical viewpoint, the system under investigation is described by a Vlasov-Poisson kinetic model with BGK-type interactions. The numerical strategy, unlike sG approximations based on a direct discretization of the system of PDEs, preserves the main physical properties of the system, including the positivity of the solution. In addition, thanks to a splitting approach and an exact representation of the collisional process, the method satisfies the asymptotic-preserving property. As a consequence, in the fluid-dynamic limit, it originates a sG particle method for the corresponding Euler-Poisson system. A collection of numerical examples, ranging from linear and nonlinear Landau damping to Sod shock tube, highlighted the spectral accuracy for smooth solutions in the random space and the validity of the present approach for problems with different space and time scales in presence of uncertainty. Future research directions
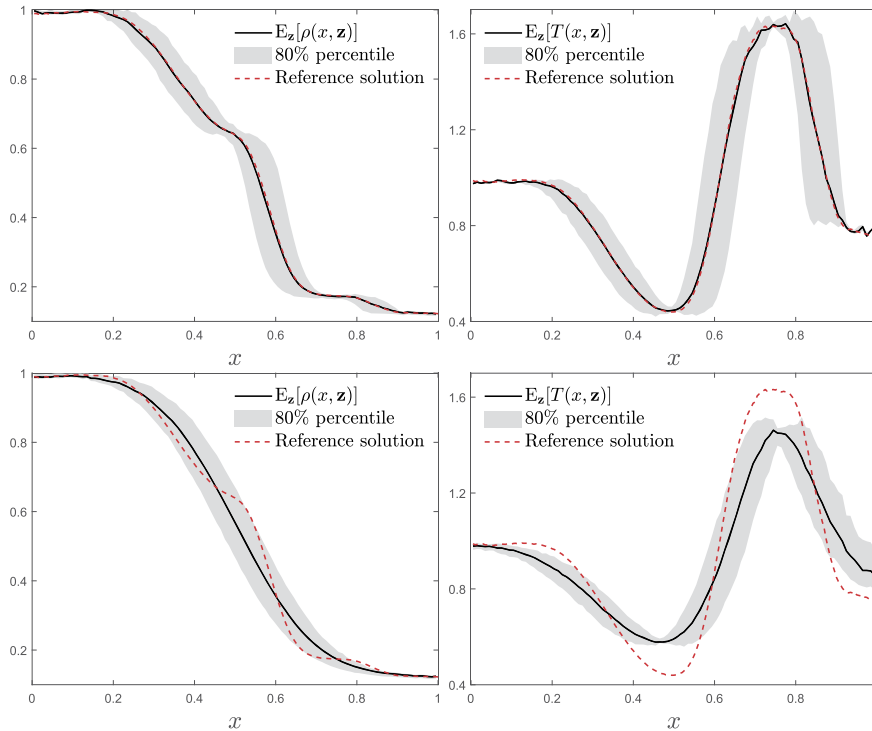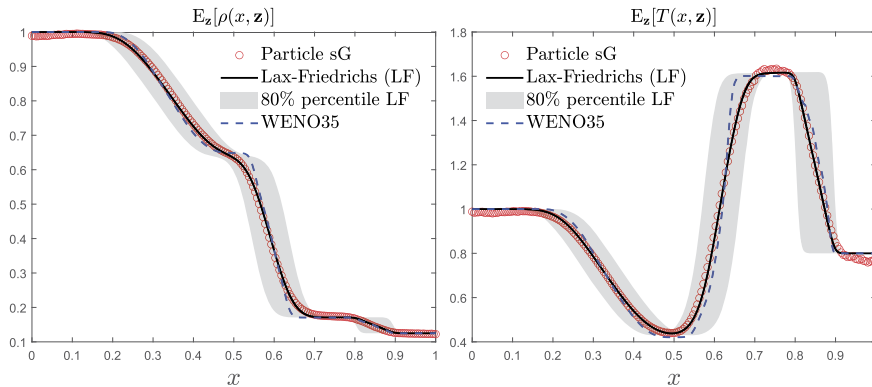
Fig. 13. Test 4: Sod shock tube. We report $\mathbb{E}_{\mathbf{z}}[\rho(x,t,\mathbf{z})]$ (left) and $\mathbb{E}_{\mathbf{z}}[T(x,t,\mathbf{z})]$ (right) for $\nu = 10^3$ (top) and $\nu = 1$ (bottom), at fixed times $t = 0.15$, for the Sod shock test with uncertain interface position. We choose $N = 10^7$, $M = 5$, $\Delta t = 0.01$. We considered the initial condition (39) with $\alpha(\mathbf{z}) = -0.05 + 0.1\mathbf{z}$, $\mathbf{z} \sim \mathcal{U}([0,1])$. Reference solution computed with $N = 10^8$ particles.

Fig. 14. Test 4: Sod shock tube. Comparison of the particle sG reference solution with Lax-Friedrichs and WENO schemes. We considered the initial condition (39) with $\alpha(\mathbf{z}) = -0.05 + 0.1\mathbf{z}$, $\mathbf{z} \sim \mathcal{U}([0,1])$. The particle solution is computed with $N = 10^8$, $M = 5$ and $\Delta t = 0.01$. Lax-Friedrichs is solved with 1500 cells and CFL number 0.1, WENO with 200 cells and CFL number 0.5. In both cases we use a stochastic collocation approach with 11 nodes.

will be devoted to the introduction of a Landau type collision term for which the application of the sG particle method is not straightforward.

CRediT authorship contribution statement

Andrea Medaglia: Conceptualization, Data curation, Investigation, Methodology, Software, Validation, Visualization, Writing – original draft, Writing – review & editing. **Lorenzo Pareschi:** Conceptualization, Formal analysis, Methodology, Supervision, Writing – original draft, Writing – review & editing. **Mattia Zanella:** Conceptualization, Formal analysis, Funding acquisition, Methodology, Project administration, Resources, Supervision, Writing – original draft, Writing – review & editing.

Declaration of competing interest

Data availability

Data will be made available on request.

Acknowledgements

Appendix A. Initial sampling

Given the initial condition $f_0(x, v, \mathbf{z})$, we consider the empirical distribution

$$f_N^0(x, v, \mathbf{z}) = \frac{m(\mathbf{z})}{N} \sum_{i=1}^N S(x - x_i^0(\mathbf{z})) \otimes S(v - v_i^0(\mathbf{z})),$$

in a way that formally $f_N^0(x, v, \mathbf{z}) \to f_0(x, v, \mathbf{z})$ as $N \to \infty$. However, as already pointed out in [39], a direct application of standard sampling techniques may be nontrivial since we have to perform a gPC projection to obtain the coefficients as presented in Section 3.2.

Algorithm 5 sG projection of the initial positions.

- Generate a set of Gaussian nodes $\{z_k\}$, for $k = 1, \ldots, K$, from the distribution of the parameters $p(\mathbf{z})$;
- discretize the spatial domain $[L_-, L_+]$ in N_ℓ equally spaced cells in a way that $x_0 = L_-, \ldots, x_\ell, \ldots, x_{N_\ell} = L_+$;
- for $k = 1$ to K:
  - compute the mass fraction of every cell $\rho_{\ell,k}^0 = \rho_\ell^0(z_k)/m(z_k)$, with $m(z_k) = \int \rho_\ell^0(z_k)dx$;
  - set $N_{\ell,k} = N\rho_{\ell,k}^0$, number of particles to sample in cell;
  - generate $N_{\ell,k}$ uniformly distributed positions $\{x_i^{0,M}(z_k)\}$ in the interval $[x_{\ell-1}, x_\ell]$, for every $\ell = 1, \ldots, N_\ell$;
  end for;
- for $h = 0, \ldots, M$:
  - compute the projections $\hat{x}_{i,h}^0$ according to (18);
  end for.

Algorithm 6 sG projection of the initial velocities.

- Generate a set of Gaussian nodes $\{z_k\}$, for $k = 1, \ldots, K$, from the distribution of the parameters $p(\mathbf{z})$;
- for $i = 1$ to N:
  - generate a reference sample of $\tilde{v}_i^0$ using suitable sampling method from the expected marginal $\mathbb{E}_{\mathbf{z}}[f_v]$ of $f_0(x, v, \mathbf{z})$ in x;
  - compute $v_i^{0,M}(z_k) = \sqrt{\frac{T(z_k)}{\tilde{T}}} \tilde{v}_i^0$ for each $k = 1, \ldots, K$, being $\tilde{T}$ the temperature of $\mathbb{E}_{\mathbf{z}}[f_v]$
  end for;
- for $h = 0, \ldots, M$:
  - compute the projections $\hat{v}_{i,h}^0$ according to (18);
  end for.

Indeed, we first need to construct a random sample $x_i^{0,M}(\mathbf{z})$, $v_i^{0,M}(\mathbf{z})$, for $i = 1, \ldots, N$ such that

$$f_N^0(x, v, \mathbf{z}) \approx \frac{m(\mathbf{z})}{N} \sum_{i=1}^N S(x - x_i^{0,M}(\mathbf{z})) \otimes S(v - v_i^{0,M}(\mathbf{z})),$$

where $x_i^{0,M}(\mathbf{z})$ and $v_i^{0,M}(\mathbf{z})$ are given by (17). Hence, by direct integration we can compute the coefficients of the polynomial chaos expansion according to (18).

Since the integrals in the random space are approximated through a Gaussian quadrature rule, we want to generate a sample of positions and velocities in every Gauss collocation node $\{z_k\}_{k=1}^K$, in a way that

$$\hat{x}_{i,h}^0 = \int_\Omega x_i^0(\mathbf{z})\Psi_h(\mathbf{z})p(\mathbf{z})d\mathbf{z} \approx \sum_{k=1}^M x_i^{0,M}(z_k)w_k\Psi_h(z_k),$$

$$\hat{v}_{i,h}^0 = \int_\Omega v_i^0(\mathbf{z})\Psi_h(\mathbf{z})p(\mathbf{z})d\mathbf{z} \approx \sum_{k=1}^M v_i^{0,M}(z_k)w_k\Psi_h(z_k).$$

As a consequence, given $f_0(x,v,\mathbf{z})$ and $p(\mathbf{z})$, distribution of the random parameters, we desire a set of samples

$$X^1 = \{x_1^{0,M}(z_1),\ldots,x_N^{0,M}(z_1)\},\ \ldots,\ X^K = \{x_1^{0,M}(z_K),\ldots,x_N^{0,M}(z_K)\}$$
$$V^1 = \{v_1^{0,M}(z_1),\ldots,v_N^{0,M}(z_1)\},\ \ldots,\ V^K = \{v_1^{0,M}(z_K),\ldots,v_N^{0,M}(z_K)\},$$

such that $\{x_i^{0,M}(z_k), v_i^{0,M}(z_k)\}$, for $k=1,\ldots,K$, represent the different realizations of the same i-th particle $\{x_i^{0,M}(\cdot), v_i^{0,M}(\cdot)\}$. We observe also that we can sample independently positions and velocities since the initial distribution functions we considered are tensorised.

At the numerical level, one possible strategy in one-dimension is to sample X^k and V^k independently with respect to the nodes z_k, with any sampling method, and then to sort positions and velocities for any $k=1,\ldots,K$. In higher dimensions, the ordering technique is not possible and we need to solve an assignment problem in order to link particles. In this work, we focused on the 1D case, and we adopted the following techniques. To observe the physical phenomena presented in Section 4 we need to sample the density $\rho_0(\mathbf{z})$ carefully by reducing statistical fluctuations. To this aim, we adopted a stratified sampling method in each Gaussian node by sorting the vectors X^k for every k at the end.

Note that, if we consider continuous probability distributions with uncertainties in the variance, e.g. a Maxwellian with uncertain temperature, we can overcome the sorting method thanks to the scaling property of the second order moment (see [39]).

References

[1] P. Andries, K. Aoki, B. Perthame, A consistent BGK-type model for gas mixtures, J. Stat. Phys. 106 (2002) 993–1018.
[2] P.L. Bhatnagar, E.P. Gross, M. Krook, A model for collision processes in gases. I. Small amplitude processes in charged and neutral one-component systems, Phys. Rev. 94 (3) (1954) 511.
[3] R. Caflisch, C. Wang, G. Dimarco, B. Cohen, A. Dimits, A hybrid method for accelerated simulation of Coulomb collisions in a plasma, Multiscale Model. Simul. 7 (2) (2008) 865–887.
[4] M. Campos-Pinto, E. Sonnendrücker, A. Friedman, D.P. Grote, S.M. Lund, Noiseless Vlasov–Poisson simulations with linearly transformed particles, J. Comput. Phys. 275 (2014) 236–256.
[5] J.A. Carrillo, J. Hu, L. Wang, J. Wu, A particle method for the homogeneous Landau equation, J. Comput. Phys. X 7 (2020) 100066.
[6] J.A. Carrillo, S. Jin, Y. Tang, Random batch particle methods for the homogeneous Landau equation, Commun. Comput. Phys. 31 (4) (2022) 997–1019.
[7] J.A. Carrillo, L. Pareschi, M. Zanella, Particle based gPC methods for mean-field models of swarming with uncertainty, Commun. Comput. Phys. 25 (2) (2019) 508–531.
[8] J.A. Carrillo, M. Zanella, Monte Carlo gPC methods for diffusive kinetic flocking models with uncertainties, Vietnam J. Math. 47 (4) (2019) 931–954.
[9] E. Chacon-Golcher, S.A. Hirstoaga, M. Lutz, Optimization of Particle-In-Cell simulations for Vlasov–Poisson system with strong magnetic field, ESAIM Proc. 53 (2016) 177–190.
[10] F.F. Chen, Introduction to Plasma Physics and Controlled Fusion, 2nd edition, Plenum Press, New York and London, 1974.
[11] S.W. Chung, S.D. Bond, E.C. Cyr, J.B. Freund, Regular sensitivity computation avoiding chaotic effects in particle-in-cell plasma methods, J. Comput. Phys. 400 (2020) 108969.
[12] A. Crestetto, N. Crouseilles, M. Lemou, Kinetic/fluid micro-macro numerical schemes for Vlasov-Poisson-BGK equation using particles, Kinet. Relat. Models 5 (4) (2012) 787–816.
[13] N. Crouseilles, F. Filbet, Numerical approximation of collisional plasmas by high order methods, J. Comput. Phys. 201 (2) (2004) 546–572.
[14] D. Dai, Y. Epshteyn, A. Narayan, Hyperbolicity-preserving and well-balanced stochastic Galerkin method for two-dimensional shallow water equations, J. Comput. Phys. 452 (2022) 110901.
[15] B. Després, G. Poëtte, D. Lucor, Robust uncertainty propagation in systems of conservation laws with the entropy closure method, in: Uncertainty Quantification in Computational Fluid Dynamics, Springer, 2013, pp. 105–149.
[16] G. Dimarco, R. Caflisch, L. Pareschi, Direct simulation Monte Carlo schemes for Coulomb interactions in plasmas, Commun. Appl. Ind. Math. 1 (1) (2010) 72–91.
[17] G. Dimarco, Q. Li, L. Pareschi, B. Yan, Numerical methods for plasma physics in collisional regimes, J. Plasma Phys. 81 (1) (2015) 1–31.
[18] G. Dimarco, L. Mieussens, V. Rispoli, An asymptotic preserving automatic domain decomposition method for the Vlasov-Poisson-BGK system with applications to plasmas, J. Comput. Phys. 274 (2014) 122–139.
[19] G. Dimarco, L. Pareschi, Numerical methods for kinetic equations, Acta Numer. 23 (2014) 369–520.
[20] G. Dimarco, L. Pareschi, Multiscale variance reduction methods based on multiple control variates for kinetic equations with uncertainties, Multiscale Model. Simul. 18 (1) (2020) 351–382.
[21] Z. Ding, S. Jin, Random regularity of a nonlinear Landau damping solution for the Vlasov-Poisson equations with random inputs, Int. J. Uncertain. Quantificat. 9 (2) (2019) 123–142.

[22] F. Filbet, L. Pareschi, A numerical method for the accurate solution of the Fokker-Planck-Landau equation in the nonhomogeneous case, J. Comput. Phys. 179 (1) (2002) 1–26.

[23] F. Filbet, L.M. Rodrigues, Asymptotically stable particle-in-cell methods for the Vlasov–Poisson system with a strong external magnetic field, SIAM J. Numer. Anal. 54 (2) (2016) 1120–1146.

[24] F. Filbet, E. Sonnendrücker, Comparison of Eulerian Vlasov solvers, Comput. Phys. Commun. 150 (3) (2003) 247–266.

[25] F. Filbet, E. Sonnendrücker, P. Bertrand, Conservative numerical schemes for the Vlasov equation, J. Comput. Phys. 172 (1) (2001) 166–187.

[26] R.W. Hockney, J.W. Eastwood, Computer Simulation Using Particles, McGraw Hill International Book Co., 1981.

[27] J. Hu, S. Jin, R. Shu, A stochastic Galerkin method for the Fokker-Planck-Landau equation with random uncertainties, in: Theory, Numerics and Applications of Hyperbolic Problems. Ilumerics and Applications of Hyperbolic Problems. II, in: Springer Proc. Math. Stat., vol. 237, Springer, Cham, 2018, pp. 1–19.

[28] J. Hu, L. Pareschi, Y. Wang, Uncertainty quantification for the BGK model of the Boltzmann equation using multilevel variance reduced Monte Carlo methods, SIAM/ASA J. Uncertain. Quantificat. 9 (2) (2021) 650–680.

[29] L.D. Landau, On the vibrations of the electronic plasma, J. Phys. 10 (1) (1965) 25–34.

[30] C. Liu, K. Xu, A unified gas kinetic scheme for continuum and rarefied flows V: multiscale and multi-component plasma transport, Commun. Comput. Phys. 22 (5) (2017) 1175–1223.

[31] C.J. McKinstrie, R.E. Giacone, E.A. Startsev, Accurate formulas for the Landau damping rates of electrostatic waves, Phys. Plasmas 6 (1999) 463–466.

[32] A. Medaglia, A. Tosin, M. Zanella, Monte Carlo stochastic Galerkin methods for non-Maxwellian kinetic models of multiagent systems with uncertainties, Part. Differ. Equ. Appl. 3 (2022) 51.

[33] L. Pareschi, An introduction to uncertainty quantification for kinetic equations and related problems, in: Trails in Kinetic Theory: Foundational Aspects and Numerical Methods, in: SEMA SIMAI Springer Ser., vol. 25, Springer, Cham, 2021, pp. 141–181.

[34] L. Pareschi, G. Russo, An introduction to Monte Carlo method for the Boltzmann equation, ESAIM Proc. 10 (2001) 35–75.

[35] L. Pareschi, G. Russo, Time relaxed Monte Carlo methods for the Boltzmann equation, SIAM J. Sci. Comput. 23 (4) (2001) 1253–1273.

[36] L. Pareschi, G. Russo, G. Toscani, Fast spectral methods for the Fokker-Planck-Landau collision operator, J. Comput. Phys. 165 (1) (2000) 216–236.

[37] L. Pareschi, G. Toscani, Interacting Multiagent System: Kinetic Equations and Monte Carlo Methods, Oxford University Press, 2013.

[38] L. Pareschi, S. Trazzi, Numerical solution of the Boltzmann equation by time relaxed Monte Carlo (TRMC) methods, Int. J. Numer. Methods Fluids 48 (9) (2005) 947–983.

[39] L. Pareschi, M. Zanella, Monte Carlo stochastic Galerkin methods for the Boltzmann equation with uncertainties: space-homogeneous case, J. Comput. Phys. 423 (2020) 1098–1120.

[40] G. Poëtte, A gPC-intrusive Monte-Carlo scheme for the resolution of the uncertain linear Boltzmann equation, J. Comput. Phys. 385 (2019) 135–162.

[41] J.A. Rossmanith, D.C. Seal, A positivity-preserving high-order semi-lagrangian discontinuous Galerkin scheme for the Vlasov–Poisson equations, J. Comput. Phys. 230 (16) (2011) 6203–6232.

[42] C.-W. Shu, High order weighted essentially nonoscillatory schemes for convection dominated problems, SIAM Rev. 51 (1) (2009) 82–126.

[43] R. Shu, S. Jin, A study of Landau damping with random initial inputs, J. Differ. Equ. 266 (4) (2019) 1922–1945.

[44] G.A. Sod, A survey of several finite difference methods for systems of nonlinear hyperbolic conservation laws, J. Comput. Phys. 27 (1) (1978) 1–31.

[45] E. Sonnendrücker, Numerical Methods for the Vlasov Equations, Lecture Notes, 2013.

[46] G. Strang, On the construction and comparison of difference schemes, SIAM J. Numer. Anal. 5 (3) (1968) 506–517.

[47] C. Villani, Landau damping, in: Numerical Models for Fusion, in: Panor. Synthèses, vol. 39/40, Soc. Math. France, Paris, 2013, pp. 237–326.

[48] T. Xiao, M. Frank, A stochastic kinetic scheme for multi-scale plasma transport with uncertainty quantification, J. Comput. Phys. 432 (2021) 110–139.

[49] D. Xiu, Numerical Methods for Stochastic Computations, Princeton University Press, 2010.

[50] D. Xiu, G.E. Karniadakis, The Wiener–Askey polynomial chaos for stochastic differential equations, SIAM J. Sci. Comput. 24 (2) (2002) 619–644.

[51] C. Zhang, I.M. Gamba, A conservative scheme for Vlasov Poisson Landau modeling collisional plasmas, J. Comput. Phys. 340 (2017) 470–497.